Chapter 11

Spin-Resolved Photoemission from Nonmagnetic Metals and Adsorbates

U. Heinzmann and G. Schonhense

Fakultät für Physik, Universität Bielefeld,
4800 Bielefeld 1, FRG
Fritz-Haber-Institut der MPG, 1000 Berlin 33, FRG

11.1 Introduction

The concept of polarized photoelectrons ejected by circularly polarized light has been introduced by Fano (1969). One year later the "Fano-effect" was experimentally confirmed for free Cs atoms (Heinzmann et al. 1970). Spin-orbit interaction is the essential mechanism leading to a spin orientation of photoelectrons with degrees of polarization of up to 100 %. Optical transitions with σ-light induce an anisotropic distribution of the m_j sublevels of the final-state wavefunction, owing to the selection rules for electric dipole transitions (e.g. $\Delta m_j = +1$ for σ^+-light).

In solids, optical pumping using circularly polarized light has been studied by means of nuclear magnetic resonance by Lampel (1968). The first polarized photoelectrons emitted from nonmagnetic solids by σ-light have been observed for evaporated polycrystalline Cs films (Heinzmann et al. 1972) and a few years later the famous results for GaAs (Pierce and Meier 1976) initiated a number of systematic investigations of single-crystal semi-conductors (cf. chapter 10) and metals. A theoretical treatment for solid Cs was performed by Koyama and Merz (1975). Later, Reyes and Helman (1977), Feder (1977 and 1978), Borstel and Wöhlecke (1981) have established the theoretical framework, which was applied to a number of single-crystal faces.

Up to 1984 experimental analysis of the electron-spin polarization (ESP) in photoionization and photoemission using circularly polarized light was restricted to angle integrated measurements without resolution of the kinetic energy of the photoelectrons ejected; that type of experiment has been performed in detail for many free atoms and molecules (see for example Heinzmann 1980a and references therein, Heinzmann et al. 1981) as well as different solids. With the development of the new German dedicated electron storage ring for synchrotron radiation, BESSY, in Berlin, a light source of circularly polarized vacuum ultraviolet (vuv) radiation with sufficiently high intensity

has become available, making angle- and energy-resolved spin-polarization transfer studies from circularly polarized radiation onto photoelectrons feasible. These measurements have been performed with free atoms, with a solid-state system as well as with atoms adsorbed on solid surfaces (as discussed in the following sections 11.2, 11.3 - 5, 11.6 - 7, respectively). The new technique extends the photon energy range beyond 10 eV, where conventional methods for producing circularly polarized radiation break down because no transparent or even double refracting material exists.

The experimental technique used is briefly presented in section 11.2.1. The measured data of photoemission with subsequent ESP analysis provides a quantitative experimental characterization of the symmetries (angular momentum quantum numbers) of the electron bands (atomic or ionic eigenstates) involved as discussed in sections 11.3 and 11.6. This becomes especially important for critical points of the energy bands and in regions, where hybridization effects play a dominant role, as discussed in 11.4. Besides the presentation of experimental results it is also the purpose of this chapter to demonstrate that the angle- and spin-resolved photoelectron spectroscopy is becoming a powerful tool to build a quantitative bridge from the atoms via the molecules and via the adsorbates to the three-dimensional crystal for the study of the electronic states and the structure of matter. A special attempt is the study of atomic effects persisting in the solid state and the adsorbate. In atomic photoionization similar measurements yield a set of parameters which characterize the photoemission process quantummechanically completely: they allow the determination of all dipole matrix elements and all phase-shift differences of the final-state wavefunctions (Heinzmann 1980a, b). To extend this to more complicated systems like solid metals and adsorbates is the pronounced goal of the running experiments.

11.2 Energy-, Angle- and Spin-Resolved Photoelectron Emission Technique

11.2.1 Experimental

The main components of the two apparatus built at BESSY in Berlin - one for studies of atomic photoionization (Heckenkamp et al. 1984) and one for photoemission experiments with solid surfaces (Eyers et al. 1984) and adsorbates (Schönhense et al. 1985) - are briefly discussed here. The synchrotron radiation is dispersed by a 6.5 m N.I. UHV monochromator of the Gillieson type (Eyers et al. 1983) with the electron beam in the storage ring being the virtual entrance slit. A spherical mirror and a plane holographic grating (1200 or 3600 lines/mm) form a 1 : 1 image of the tangential point in the exit slit. With a slit width of 2 mm a bandwidth of 0.5 nm has been achieved. Apertures movable in vertical direction are used to select radiation emitted above and below the storage ring plane, which has positive or negative helicity, respectively. In the plane the synchrotron radiation is linearly polarized. The optical degrees of polarization of the synchrotron radiation have been measured by Heckenkamp et al. (1984) by means of a rotatable four mirror analyzer (Heinzmann 1980b). Fig. 1 shows the results of the circular polarization P_{circ} and the linear polarization P_{lin} as functions of the vertical angle

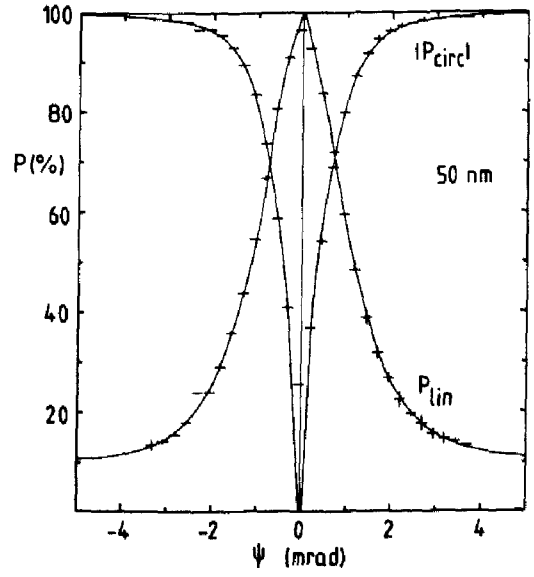

Fig. 1: Degree of circular and linear polarization P_{circ} and P_{lin}, respectively, of vuv synchrotron radiation emitted from the BESSY storage-ring plane as function of the vertical angle ψ (± 0.1 mrad) as measured by Heckenkamp et al. (1984).

ψ ($\pm$ 0.1 mrad). The solid lines which represent the theoretical predictions show excellent agreement with the experimental results demonstrating a complete linear polarization and a vanishing circular polarization of radiation emitted in the plane of the BESSY storage ring. Under the conditions of radiation accepted in the vertical angular range from 1 to 5 mrad out of the storage ringe plane, a photon flux of 10^{11} to 10^{12} photons s^{-1} with a degree of circular polarization P_{circ} = 93 % passes the monochromator exit slit and hits the photo-target under normal incidence producing photoelectrons in a region free of electric or magnetic fields.

As indicated in the schematic diagram of the apparatus shown in Fig. 2, the sample is cleaned by ion bombardment, heating in oxygen, and flashing; it is characterized by LEED and Auger-electron spectroscopy in a separate preparation chamber. The crystal on top of a manipulator moveable between preparation and photoemission chamber, can be cooled by use of a temperature—controlled liquid He-cryostat to temperatures of less than 40 K. Adsorbates are introduced via a doser nozzle which kept the background pressure below 10^{-9} mbar (base pressure $5 \cdot 10^{-11}$ mbar), allowing the continuous monitoring of the photoelectron spectra and LEED patterns as function of the coverage.

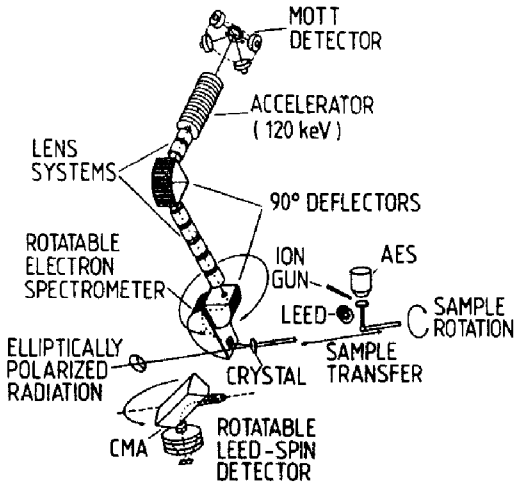

Fig. 2: Schematic diagram of the apparatus, built up at BESSY.

The photoelectrons are analyzed with respect to their kinetic energy either by a cylindrical-mirror analyzer followed by a *LEED spin detector* (Oepen et al. 1985) or by a simulated hemispherical spectrometer followed by a *UHV-Mott detector* (Eyers et al. 1984, Schönhense et al. 1985). Both electron spectrometers moveable up and down into the measuring and waiting position are rotatable about two axes which are perpendicular to the photon momentum at the crystal. These rotation axes being different with respect to the light-polarization ellipse will become important in studies of off-normal photoemission (cf. 11.5) where both spin analyzers shown in Fig. 2 complement each other.

In the upper system shown in Fig. 2 the photoelectrons analyzed with respect to their kinetic energy are directed by a 90° electrostatic deflection along the axis of rotation of the electron spectrometer. After a second deflection they are accelerated to 120 keV and scattered at the gold foil of the Mott detector for the spin-polarization analysis. Instrumental asymmetries have been eliminated by taking advantage of the reversal of the light helicity (typically each minute) as well as by use of four additional detectors in forward scattering directions (Heinzmann 1978) in the Mott detector (not shown in Fig. 2). Count rates of more than $10^3 s^{-1}$ have been obtained in the detectors for the spin analysis; the angular and energy resolution of the electron spectrometer was ±3° and 90 meV (Schönhense et al. 1985), respectively.

11.2.2 The "Complete" Photoionization Study

The reaction plane of symmetry for an angle- and spin-resolved photoionization process of an *unpolarized atom* or *unoriented molecule* using circularly polarized radiation is shown in Fig. 3. Because the momentum of the photon is negligibly small compared with the momentum of the photoelectron (valid in nonrelativistic approximation for photon energies ≦100 eV) there is a forward-backward symmetry in the reaction plane of Fig. 3. It also makes no difference whether right handed circularly polarized radiation comes from the left or left handed comes from the right. The rotational symmetry around the direction of the photon momentum causes both ESP components perpendicular to the photon spin to vanish for photoelectron emission angles $\theta = 0, \pi/2, \pi$. This is shown in Fig. 4, where the angle dependences of intensity $I(\theta)$ and spin-polarization components are shown for a certain atomic photoionization process (xenon), which has been simultaneously resolved with respect to all relevant variables i.e.: radiation wavelength 80 nm, radiation polarization σ^+, electron emission angle θ, electron kinetic energy corresponding to the final ionic state $Xe^+ {}^2P_{1/2}$, the 3 components of the ESP vector $\vec{P}(\theta)$: $P_\perp(\theta)$ perpendicular to the reaction plane, $A(\theta)$ parallel to the photon spin, $P_p(\theta)$ perpendicular to the photon spin but in the reaction plane.

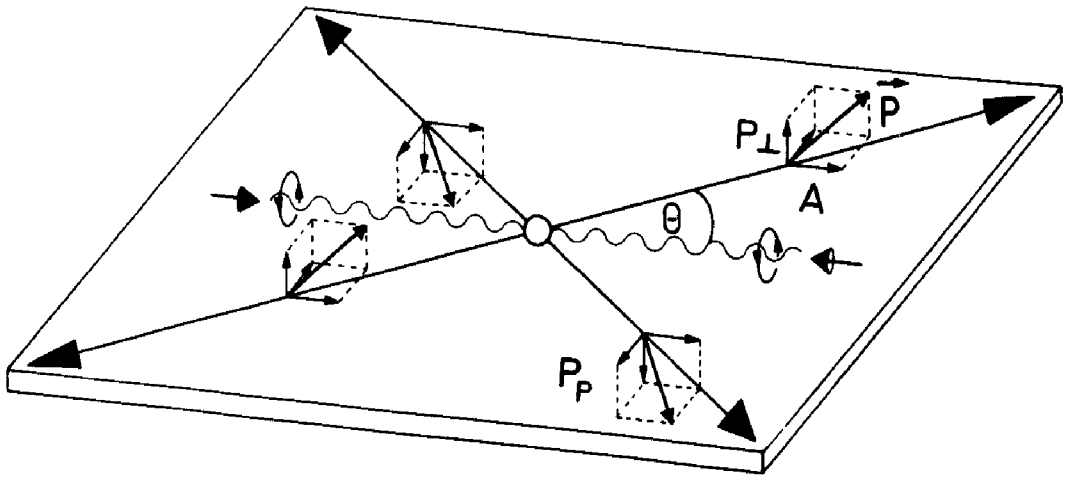

Fig. 3: Photoionization reaction plane in the case of circularly polarized radiation used.

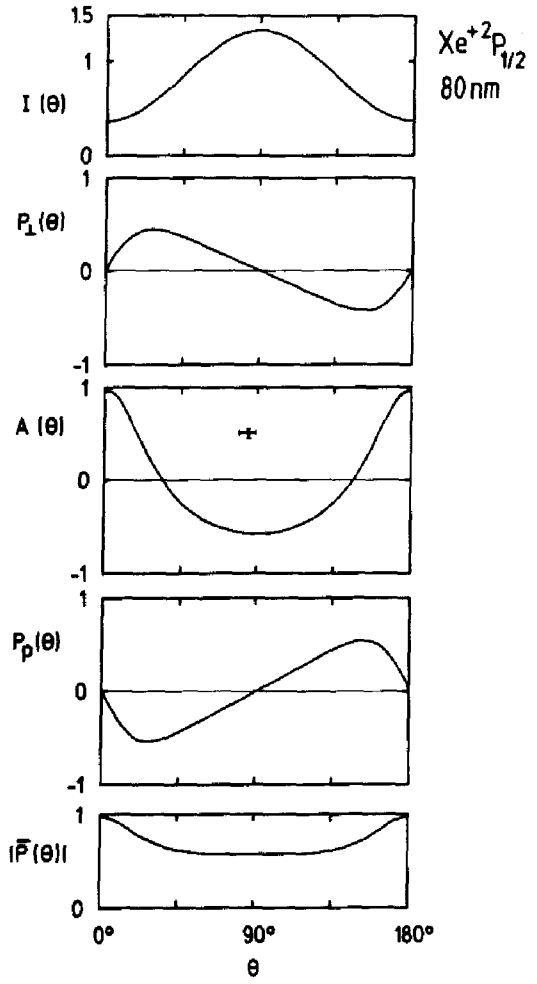

Fig. 4: Fit-curves of the experimental results (the size of a typical error-bar cross is given in the middle part) describing the angular dependences of the photoelectron intensity $I(\theta)$, of the 3 components and the length of the ESP vector for photoionization of Xe atoms at 80 nm; the photoelectrons leave the ion in the $^2P_{1/2}$ state.

The curves in Fig. 4 are fits to the experimental points (Heckenkamp et al. 1984 and 1985) in accordance with the theoretical predictions by Cherepkov (1973) and Lee (1974).

$A(\theta)$ and $P_p(\theta)$ vanish, if linearly polarized or unpolarized instead of circularly polarized radiation is used (Heinzmann et al. 1979a, Schönhense 1980). All five curves in Fig. 4 show a reflection symmetry with respect to $\theta = \pi/2$, but $P_\perp(\theta)$ and $P_p(\theta)$ with changing sign. Thus, the polarizations of opposite sign cancel one another, if the photoelectrons ejected are extracted by an electric field regardless of their direction of emission. The only non-vanishing component of the spin polarization in an angle-integrated measurement is A (Fano effect). It is also worth noting that within the error limits the photoelectrons emitted into the forward direction $\theta = 0$ have been found by Heckenkamp et al. (1984) to be completely spin polarized (Fig. 4 middle part). This complete ESP in forward direction parallel to the photon spin as well as the fact that the electron polarization is proportional to the degree of photon polarization if partly polarized radiation is used, allows to characterize the process by the phrase "spin-polarization transfer" from spin polarized photons onto photoelectrons.

The bottom part of Fig. 4 demonstrates that the length of the ESP vector never vanishes as function of the emission angle θ. This can be generalized by the experimentally confirmed rule, that in an angular resolved photoemission experiment on atoms, molecules, adsorbates or solids it is very common rather than exceptional to get spin polarized photoelectrons.

Using the results in Fig. 4 and their energy dependences (Heckenkamp et al. 1984 and 1985), all dipole matrix elements and phase-shift differences of the continuum wavefunctions describing the photoelectron emission from xenon atoms could be determined separately. Similar results of this quantummechanically complete experimental characterization have also been obtained in photoionization of mercury atoms (Schäfers et al. 1985).

11.3 Symmetry-Resolved Bandmapping of Pt(111)

Pt(111) was chosen in the experiments (Eyers et al. 1984 and 1985, Oepen et al. 1985) because of its high atomic number and its unreconstructed surface and the fact that several relativistic bandstructure calculations exist.

11.3.1 Relativistic Bandstructure

Fig. 5 shows the non-self-consistent fully relativistic augmented plane wave (RAPW) bandstructure of Andersen (1970) extended to energies up to 22 eV above the Fermi level E_F by Borstel (Eyers et al. 1984). It is in excellent quantitative agreement with a recent corresponding self-consistent bandstructure calculation of Eckardt and Noffke (Leschik et al. 1984). In the following the symmetry properties of the bands along the Λ-direction in $\vec{k}$ space are used, numbered at L from 1 to 10 with increasing energy. In normal emission the dominant direct interband transitions are those occuring from the

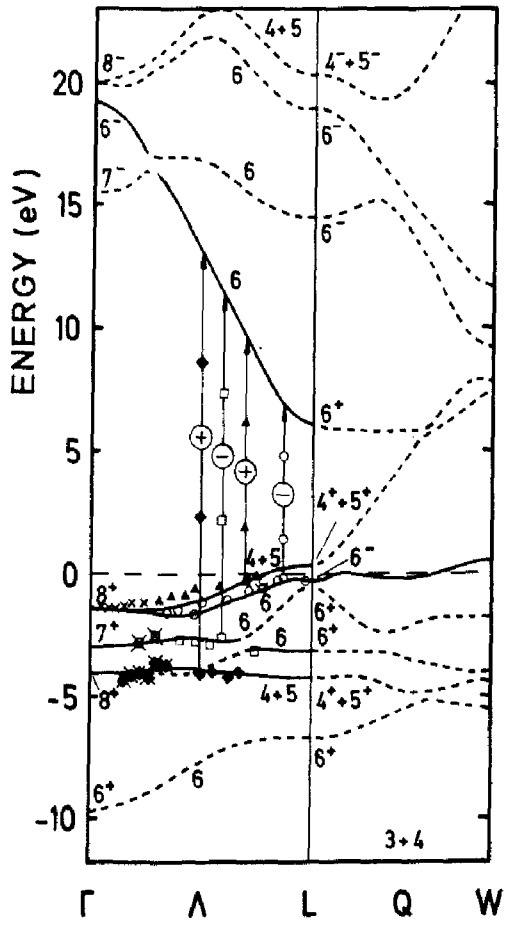

Fig. 5: Symmetry-resolved bandmapping of Pt in comparison with the calculated bandstructure. The mapping points (filled for positive and open for negative polarizations) have been obtained by a combination of intensity and polarization results of photoelectrons, partly shown in Fig. 6. For photon energies > 20 eV, bandmapping using a free-electron parabola as final state yields the crosses (from Eyers et al. 1984).

initial d-bands (Nos. 2 – 6) with the symmetries Λ_{4+5}^3, Λ_6^3, Λ_6^1, Λ_6^3, Λ_{4+5}^3 to the totally symmetric final-state band No. 7 of type Λ_6. Since a transition $\Lambda_6^1 \rightarrow \Lambda_6^1$ is forbidden for normally incident light and without hybridization (11.4), only 4 direct transitions from the initial states Λ_{4+5}^3, Λ_6^3 occur (which evolve from the two nonrelativistic doublets Λ_3 and which are drawn as solid line in Fig. 5).

11.3.2 Spin-Resolved Photoelectron Spectra and Bandmapping

A few examples of photoelectron energy distribution curves (EDC) and corresponding photoelectron spinpolarizations (ESP) measured by Eyers et al. (1984) are shown in Fig. 6.

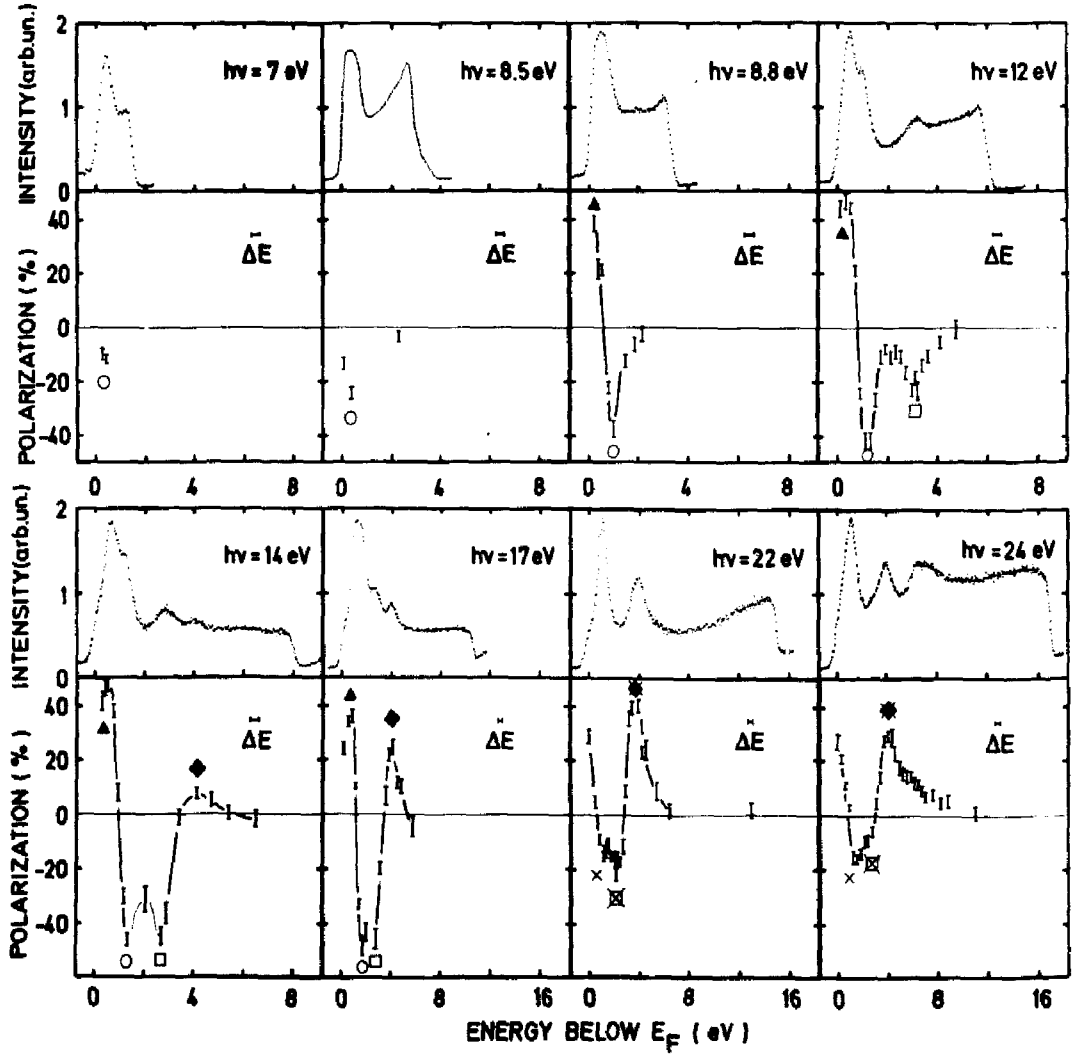

Fig. 6: Photoemission of Pt(111) (normal incidence and emission) using circularly polarized vuv radiation; photoelectron EDC (with respect to Fermi energy), upper parts; photoelectron polarization measured and normalized to a complete light polarization, lower parts. The symbols at the polarization peaks correspond to those in Fig. 5 (from Eyers et al. 1984).

The selection rules for the production of polarized electrons in cubic crystals have been discussed by Wöhlecke and Borstel (1981); they predicted a positive and a negative ESP for a transition of type $\Lambda_{4+5}^3 \rightarrow \Lambda_6^1$ and $\Lambda_6^3 \rightarrow \Lambda_6^1$, respectively.

The first direct transition (open circle) occurs near L from band No. 5 for a photon energy of about 6.5 eV as predicted in Fig. 5. Fig. 6 shows the corresponding spectrum for $h\nu$ = 7.0 eV with the expected negative sign of the ESP. The low ESP may be explained by a small transition probability near L and a strong admixture of essentially unpolarized electrons from non $k_\perp$-conserving transitions possibly originating from band No. 5 along Q, which has a very high total density of states just below the Fermi energy (Mueller et al. 1971).

For increasing energy the probability of direct transitions $5 \rightarrow 7$ increase moving away from the L point. Thus the negative ESP is seen more clearly for a photon energy of 8.5 eV. Photoemission from the upper Λ_{4+5}^3 band (No. 6) sets in close to 8.8 eV with a positive polarization, as expected. If $h\nu$ is increased towards 14 eV, the two doublet bands 3 and 2 (Λ_6^3, Λ_{4+5}^3) produce an ESP of the expected sign. The sequence of spectra in Fig. 6 demonstrates how the signs of the spin polarization lead to an unequivocal characterization of the symmetries of the initial bands. For higher photon energies the interpretation of the data within the ground-state bandstructure becomes more and more inadequate because of the importance of self-energy corrections in the final states.

As shown in Fig. 6 less than ±100 % predicted ESP has been measured, this is due to theoretical as well as experimental effects; the reasons are discussed in the following section.

11.3.3 Temperature Dependence

Fig. 7.a shows EDC and ESP for a photon energy of 10.6 eV in normal photoemission of Pt(111) at room temperature. The spectra clearly show two peaks with positive and negative ESP arising due to the transitions Λ_{4+5} and Λ_6 to Λ_6, respectively. As discussed in the preceding section, the polarizations, however, never exceeded ±55 % in contradiction to the theoretical predictions of ±100 % in terms of application of the group theory. Fig. 7.c shows the ESP, measured by Eyers et al. (1985), in the first two peaks of the intensity spectrum (Fig. 7.b) as function of the temperature between 30 K

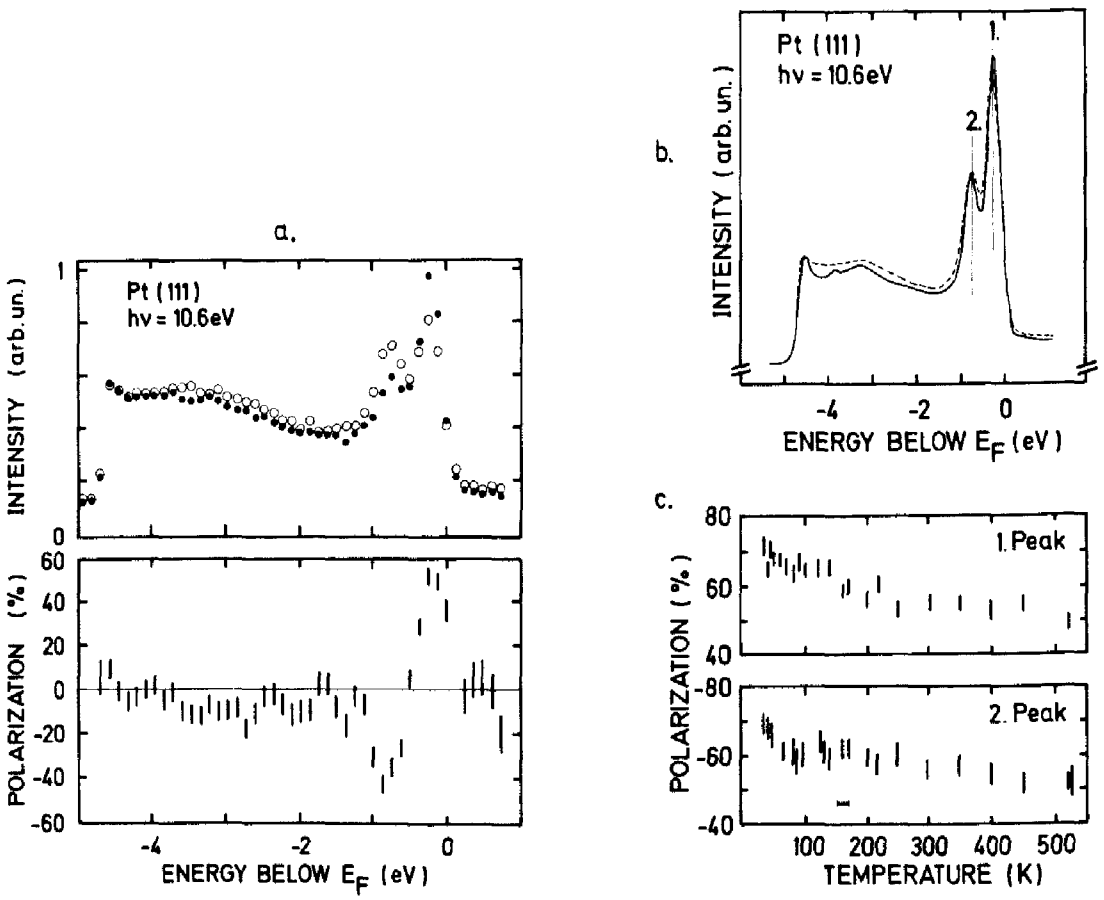

Fig. 7.a: Spin-resolved photoelectron spectrum of Pt(111) (normal incidence and emission at 300 K);Upper part: intensities measured directly in the two counters of the Mott detector, solid and open circles; Lower part: electron spin polarization
Fig. 7.b: Highly resolved EDC ($\Delta E \simeq 150$ meV FWHM) of Pt(111) at 300 K (dashed line) and 40 K (solid line)
Fig. 7.c: The temperature dependence of the electron polarizations of peaks 1 and 2 (Fig. 7.b) at 10.6 eV photon energy (all from Eyers et al. 1985).

and 550 K. With decreasing temperature the ESP increases from ±50 % to more than ±70 %. This effect might be explained by a decreased emission of unpolarized electrons from the non-$k_{\perp}$-conserving transitions as discussed in 11.3.2 or other phonon assisted non-direct transitions which enhance the inelastic contributions to the direct transitions. This is also seen in the widths of the intensity peaks shown in Fig. 7.b which become smaller by about 50 meV going from 300 K to 40 K. Taking into account that electrons in the inelastic background (Fig. 7.a) are unpolarized, the ESP analysis of both direct peaks alone yields data close to ±80 % for a temperature of 30 K, which is rather close to the theoretical prediction of a complete polarization as discussed in the preceding sections.

It is worth noting that each value shown in Fig. 7.c has been obtained by Eyers et al. (1985) just after the crystal has been cooled down to the corresponding temperature. This procedure was necessary in order to work with a clean crystal, because a marked depolarization seen as a function of the time demonstrated the influence of rest-gas adsorption on the crystal surface (11.7).

11.3.4 Comparison with Quantitative Theoretical Calculations

The general situation in the theoretical treatment of the spin-resolved photoemission is discussed in detail in chapter 4.5. There are two different kinds of theories to calculate spin effects in photoemission: the first uses the 3-step model (Borstel and Wöhlecke 1982) handling the photoexcitation in the bulk, the tranportation of the photoelectrons to the surface and finally the transmission through the surface as independent processes. This way has the advantage that the sign of the ESP and thus the symmetry of the bands involved are easily correctly predicted, as discussed in detail in 11.3.2; but a quantitative prediction of the spin polarization is very rough, because the theory does not take into account finite lifetimes of the photoelectrons produced and of the holes left behind; it further uses only bound states as final states in the photoexcitation which neglects any influence of phases in coherent superpositions; it means that in the photoexcitation there is for example no ESP component $P_{\perp}$ perpendicular to the reaction plane as discussed in 11.2.2. Because the crystal has to be infinite in 3 dimensions, adsorbate-induced effects cannot be discussed quantitatively of course.

The second way to calculate spin-resolved photoemission is the relativistic one-step model. It uses LEED-states as final states and takes into account a priori the lifetime of the photoelectrons, coherent superpositions and a semi-infinite crystal. It has the disadvantage that interpretations in terms of band structures are difficult especially if finite lifetimes of the holes are also taken into account a priori. Very recently, two first one-step photoemission calculations including spin effects have been performed for Pt(111) and published (Ackermann and Feder 1985, Ginatempo et al. 1985) both taking into account the hole lifetimes a posteriori by convoluting the photocurrent density matrix with a Lorentzian. This treats the one-step photoemission exactly close to the Fermi energy, but might give some discrepancies to the experimental results at higher energies due to the approximation for the assumed energy dependences of the hole lifetimes.

The agreement between experiment (Eyers et al. 1984, 1985) and the calculations by Ginatempo et al. (1985) is satisfactory if one takes the experimental data of Fig. 6 obtained at room temperature but less satisfactory if one takes into account the temperature effects discussed in 11.3.3 and shown in Fig. 7. On the other hand the spin-polarization results calculated by Ackermann and Feder (1985) show good agreement with the experiment performed at low temperatures (30 K) where polarizations of more than ±70 % have been measured (Eyers et al. 1985). This is demonstrated in Fig. 8 upper part, where in the first peak A (middle part) corresponding to a transition from the Λ_{4+5} band the theoretical spin polarization is a little bit higher than the experimental one, whereas in the second peak B corresponding to a transition from Λ_6 it is vice versa: the polarization measured is higher than the calculated one (a not very often obtained behavior in spin-resolved photoemission). Usually, depolarization effects due to a non-zero energy resolution as well as an angular resolution and due to an unpolarized inelastic background in the photoelectron spectra are present in the experiment, while the theoretical results of Fig. 8 are the elastic currents only.

It seems nevertheless to be evident that the one-step theories have some freedoms of adjustable quantities (hole lifetime, imaginary potential part, inelastic contributions) in order to find a more quantitative agreement with the experimental data. To continue this procedure should be an important purpose of further theoretical investigations. Quantitative comparison of experimental spin polarizations with theory requires an exact knowledge of the experimental uncertainties, of the degree of circular light polarization and of the analyzing power and asymmetry function of the spin detector used. For the evaluation procedure of the data in Figs. 6 and 7 these "experimentally important" points have been taken into account carefully.

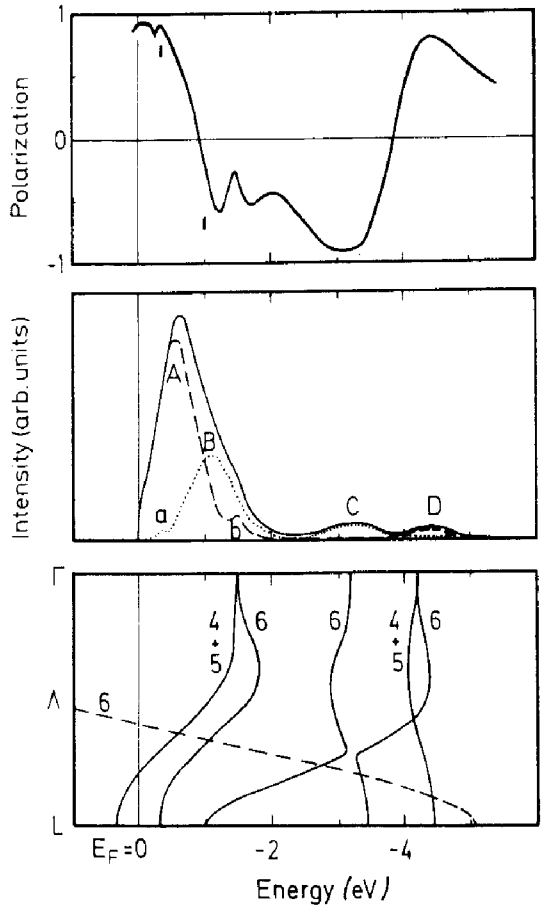

Fig. 8: Theoretical results for Pt(111) of Ackermann and Feder (1985). Lower part: Bulk band structure along ΓL for initial state (——) and for final state lowered by photon energy hν = 11 eV (---).
Middle part: Intensities I^+ (---) and I^- (•••) of elastic normal-emission photocurrent due to normally incident positive-helicity radiation (hν = 11 eV). (I^+ and I^- peaks are labelled by letters A to D and a,b).
Upper part: Spin polarization for elastic current is compared with two experimental values (error bars from Eyers et al. 1985).

11.4 Hybridization Effects and Special Regions of Energy Bands

11.4.1 The W(100) Case

Hybridization, i.e. mixing of wavefunctions with different orbital symmetries may occur as a consequence of spin-orbit interaction if the wavefunctions belong to the same double-group representation. Only in special cases can such an admixture be seen in the photoelectron intensity spectra. This happens when transitions appear which should be dipole-forbidden if the states involved were of a pure single symmetry type. For dipole-allowed transitions that simple indicator of hybridization does not work. If, however, a state is admixed which produces spins of opposite sign, the ESP of the transition is diminished as compared to the value expected for non-hybridized bands.

The capability of ESP measurements to probe the hybridization properties of conduction bands has first been experimentally verified for the W(100) direction by Zürcher et al. (1979). The theoretical framework was established by Reyes and Helman (1977) who made quantitative predictions of the ESP for photoemission from tungsten. The band structure of W along Δ is shown in Fig. 9. Dashed lines indicate the

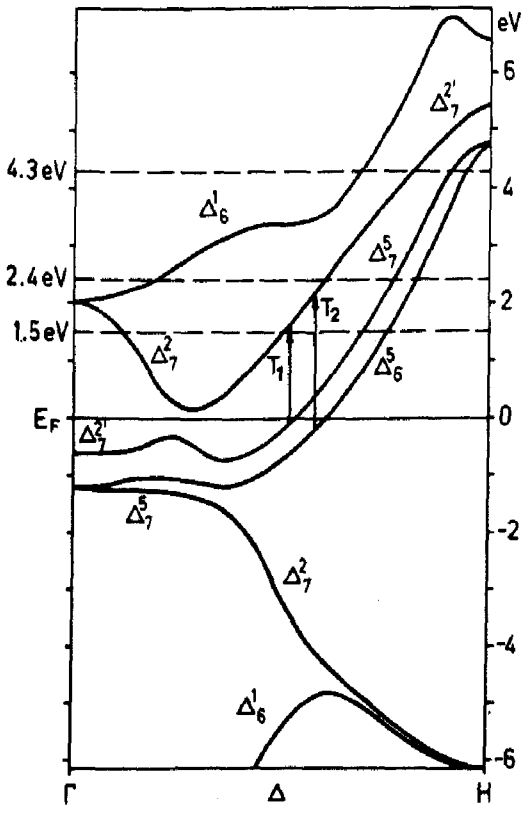

Fig. 9: Band structure of W(100) (Christensen and Feuerbacher 1974).

vacuum levels for the clean (4.3 eV) and two cesiated surfaces (2.4 and 1.5 eV). Since in this part of the Brillouin zone energy bands of different orbital symmetries are energetically rather close to each other, considerable orbital mixing due to hybridization is very likely to occur. From the dipole selection rules applied to *non-hybridized* orbitals one expects *completely polarized* photoelectrons of opposite sign for transitions T_1 and T_2 induced by circularly polarized light (Reyes and Helman 1977). However, hybridization will generally lower the ESP as illustrated in the table:

without hybridization	spins	*with* hybridization	spins
T_1: $\Delta_7^5 \rightarrow \Delta_7^{2'}$	$\downarrow$	T_1: $\Delta_7^5 + \Delta_7^{2'} + \Delta_7^2 \rightarrow \Delta_7^{2'} + \Delta_7^5 + \Delta_7^2$	$\downarrow + \uparrow$
T_2: $\Delta_6^5 \rightarrow \Delta_7^{2'}$	$\uparrow$	T_2: $\Delta_6^5 + \Delta_6^1 \rightarrow \Delta_7^{2'} + \Delta_7^5 + \Delta_7^2$	$\uparrow + \downarrow$

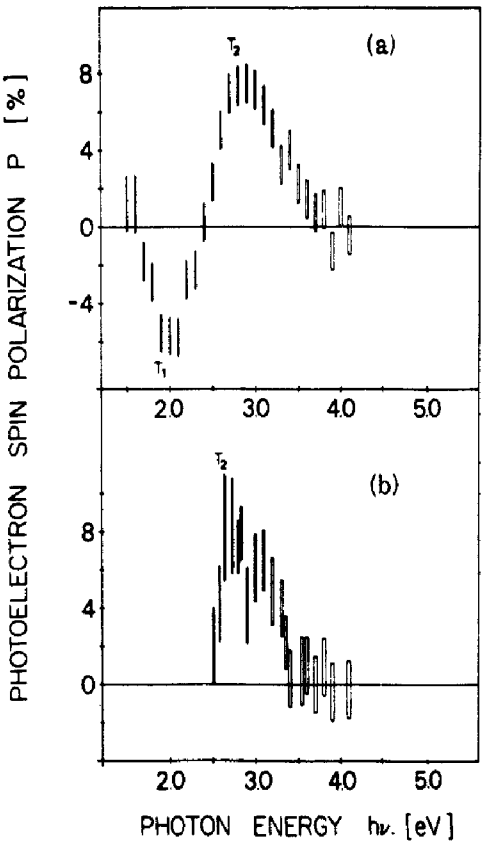

Fig. 10: ESP of the total photocurrent emitted by circularly polarized light from W(100) with photothreshold (a) 1.5 eV and (b) 2.4 eV. The extrema T_1 and T_2 arise due to the transitions indicated in Fig. 9 (Zürcher and Meier 1979).

Indeed, Zürcher et al. (1979) observed peak values of the ESP far off the theoretically predicted ±100 % as shown in Fig. 10. As discussed by the authors, depolarizing effects like contributions from off-normal emission due to the finite escape cone, a background of unpolarized electrons from surface photoemission or spin-exchange scattering at the Cs overlayer cannot explain the strongly diminished ESP. Assuming a reasonable contribution of surface emission and allowing for a small overlap of T_1 and T_2 due to lifetime broadening, the hybridization coefficients could be derived from the ESP data. For transition T_1 (T_2), the final state was estimated to be about 54 % (59 %) d-type of Δ_7^2 symmetry and 46 % (41 %) pd-type of Δ_7^5 symmetry. For the initial state corresponding to T_1 the d and pd contributions are interchanged, whereas for transition T_2 it was not possible to obtain the hybridization coefficients of the initial state from the experimental ESP data (Zürcher et al. 1979).

11.4.2 The Λ-Direction of Pt and Au

Closely related to the effects of hybridization is the question of crossings or anticrossings of energy bands. Owing to its potential for the experimental determination of bandstructure symmetries, spin-resolved photoemission is a unique tool for solving such questions. This has been demonstrated recently for platinum, where a discrepancy between theoretical bandstructure calculations could unequivocally be resolved by means of ESP measurements. The discrepancy concerns the Γ-L direction of Pt in the region 2 - 4 eV below E_F, where two relativistic calculations predicted a fundamentally different behavior: two band crossings appeared in the calculation of MacDonald et al. (1981) whereas Mackintosh (see Andersen 1970) found two anticrossings at the same points. Within the experimental uncertainty, bandmapping data (Mills et al. 1980) were compatible with both theories.

Spin- and momentum-resolved photoemission spectra of the corresponding energy regions were taken by Oepen et al. (1985) using the LEED spinpolarization detector (cf. chapter 5) and the set-up at BESSY. Fig. 11 shows for $h\nu = 13$ eV the measured ESP (a) and intensity curve

(b). As illustrated in (d), this spectrum shows just the section (dashed curve) across one of the critical regions (band Nos. 3 - 4). The general features of the spectrum have been discussed in detail in section 11.3, here we focus attention on the region around 2 - 4 eV below E_F. While in the total intensity curve the feature C appears as a single broad peak, the ESP curve and even more clearly the partial intensity curve (-) reveal structures near -2.5 eV that have to be attributed to a second peak of minor intensity (marked by arrows). Since the ESP of both peaks has the same sign, the initial states must be of the *same* symmetry; hence the two bands in question cannot cross but must form an *anticrossing* as shown in (d). Note that away from the hybridization region transitions from band 3 to the final-state band are forbidden since both have Λ_6^1 symmetry. Corresponding spectra at several other photon energies (cf. section 11.3) gave

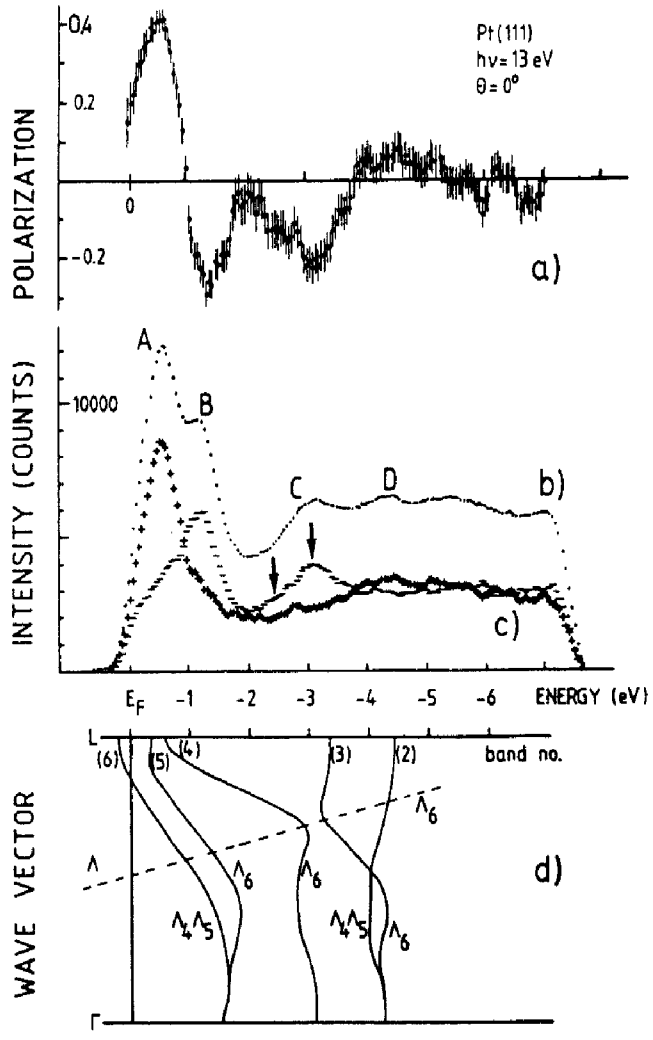

Fig. 11. Spin polarization (a), total intensity (b) and partial intensities (c) for spin parallel (+) and antiparallel (-) to the surface normal (Oepen et al. 1985).
Theoretical bandstructure of Pt along Λ (d) (after Borstel, Eyers et al. 1984) with the final-state band (dashed) being shifted by 13 eV.

evidence that band 2 must be of $\Lambda_4\Lambda_5$ symmetry while band 3 is of Λ_6 symmetry. Thus the *crossing* (at 4 eV below E_F) of the two bands of *unlike* symmetry is allowed.

The band structure of gold has attracted great interest because large discrepancies between experiments and calculations have been reported (see, e.g. Christensen 1981). Meier and Pescia (1981) studied transitions induced by circularly polarized light along the (111) direction near the L point. From the measured ESP of the total photocurrent as function of photon energy they were able to precisely determine several interband energies. The experimental energy positions of the topmost bands agree well with the relativistic band-structure calculation of Christensen and Seraphin (1971), thereby clarifying the previous controversy. The symmetry character of the bands near E_F has been unambiguously assessed. Close to the L point the top occupied band is Λ_6^1 symmetry (equivalent to band 3 of Pt, Fig. 11). The forbidden transition from this band to the Λ_6^1 final state becomes allowed by hybridization with band Λ_6^3. This admixture to the initial state wavefunction could clearly be identified due to the negative ESP ($\Lambda_6^3 \rightarrow \Lambda_6^1$) at the photothreshold.

11.5 Off-normal Photoelectron Emission

11.5.1 Surface Transmission Effects

In contrast to the ESP induced by the dipole selection rules for optical transitions with circularly polarized light, there exists another spin phenomenon in solid-state photoemission which becomes only observable in fully energy-, angle- and spin-resolved measurements. Off-normally emitted photoelectrons experience a *spin-dependent diffraction* during their transmission through the surface. The physical origin of this effect is the spin-orbit interaction in the solid, therefore a strong analogy exists to spinpolarized LEED (see chapter 6). If the excitation process produces an *unpolarized* Bloch wave (for example after excitation with unpolarized light) these electrons may acquire a nonzero ESP due to spin-dependent phase-matching conditions at the solid / vacuum interface, i.e. when going from the Bloch-spinor regime to the free-electron regime. If the excited Bloch wave is already *polarized* the effect of the surface transmission becomes more involved: in addition to changes of the ESP even intensity asymmetries occur.

The surface transmission effect in its pure appearance - the nonzero ESP after excitation by unpolarized light - was observed by Kirschner et al. (1981). Photoelectrons in tungsten were excited by Ly_α radiation from a H-discharge lamp normally incident on the 001 surface. The electrons were sampled at a polar angle of $\theta = 70°$, energy analyzed by an electron spectrometer ($E \simeq E_F$-0.5 eV) and spin analyzed by a LEED detector (see chapter 5). Fig. 12 shows the experimental data, taken in the form of azimuthal scans by rotating the crystal around its surface normal. The existence of the ESP and its structure connected to the crystal symmetry is a direct evidence of surface transmission effects (sometimes referred to as "final state ESP effects"). The quantization axis in Fig. 12 is the normal of the reaction plane spanned by incoming photon and outgoing electron. The same axis defines the well-known ESP component which occurs in photoionization of unpolarized atoms with unpolarized light (Heinzmann et

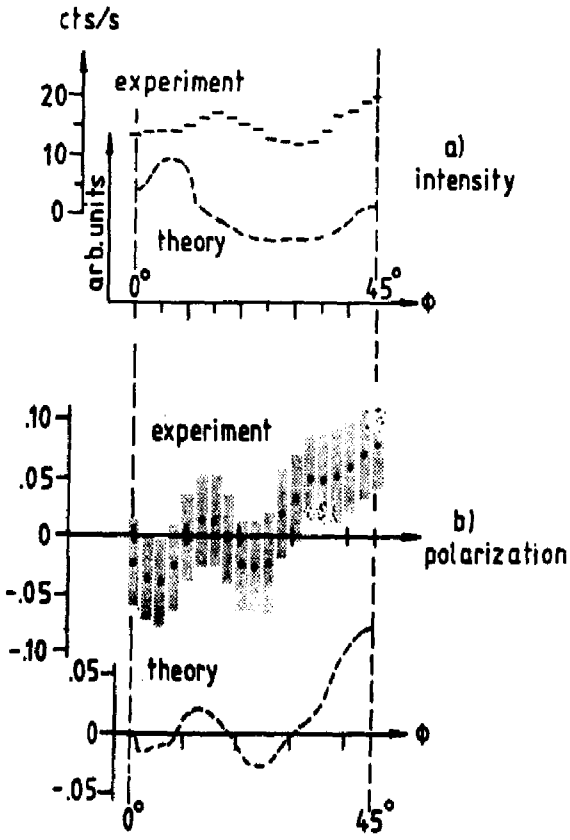

Fig. 12: Experimental and theoretical rotation diagrams (azimuthal scans) for (a) intensity and (b) ESP of photoelectrons released by *unpolarized* light from W(001); polar angle θ=70°, photon energy 10.2 eV (from Kirschner et al. 1981).

al. 1979a). Although arising under similar conditions and both being final-state effects, the physical nature of the atomic and solid-state effect is of course different: it is a consequence of quantum-mechanical interference between different photoelectron partial waves and between scattered partial waves, respectively.

The spin-dependent transmission through the surface may give rise to characteristic *intensity asymmetries* if the photoelectrons are excited by circularly (or elliptically) polarized light. In this case the electrons excited in the bulk are polarized and the transmission step depends explicitly on their spin-state. The surface can be viewed as a polarizing filter which weakens or enhances the transmitted intensity from a particular transition, depending on the sign of the ESP and hence on the helicity of the incident radiation. This is demonstrated in Fig. 13 for Pt(111). Part a) shows two intensity curves for σ^+ and σ^- light at $h\nu$ = 12 eV yielding the asymmetry shown in b). The two peaks near E_F stem from transitions from the topmost occupied band split by spin-orbit interaction, i.e. from electrons

of opposite spin orientation. When the spin-dependence of the transmission step is known, this effect offers the possibility of an experimental determination of band-structure symmetries *without* explicit ESP analysis.

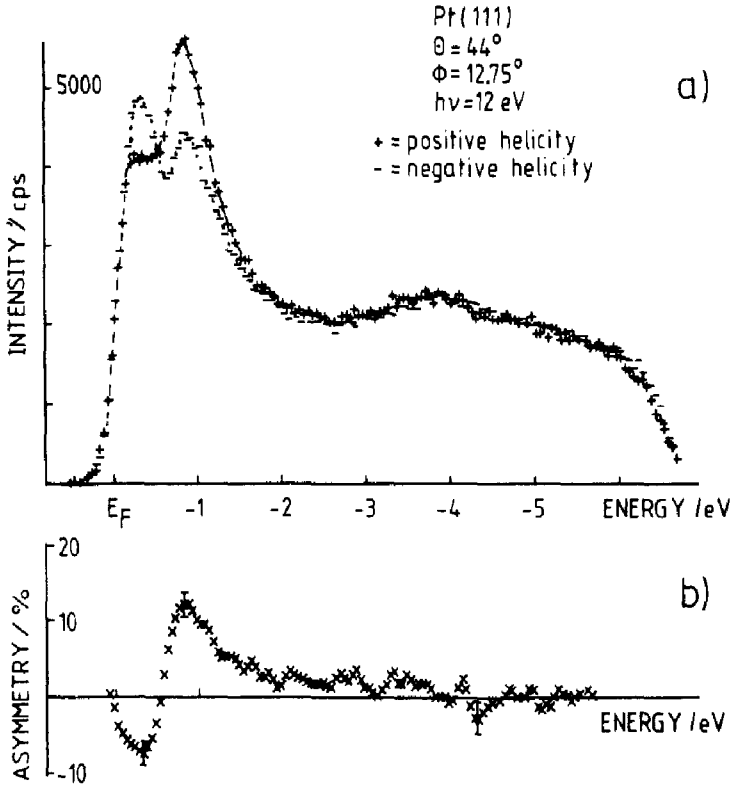

Fig. 13: Photoelectron intensity spectra and resulting asymmetry $(I^+-I^-)/(I^++I^-)$ measured for σ-light of opposite helicity. ϕ is measured from the ΓLUX mirror plane of Pt(111) (from Oepen et al. 1984).

11.5.2 Dependence of the ESP Vector on the Emission Angle

Similar to scattering of polarized electrons on free atoms (cf. Kessler 1976), the spin dependent diffraction of polarized electrons on surfaces generally changes the ESP vector in magnitude and direction. The scattering matrix depends on the electron energy and the emission angle. Oepen et al. (1985) have measured the ESP vector in the ΓLUX mirror plane of Pt(111) for different polar emission angles and several photon energies. One example is shown in Fig. 14; P_{long} and P_{trans} denote the longitudinal and transversal ESP components

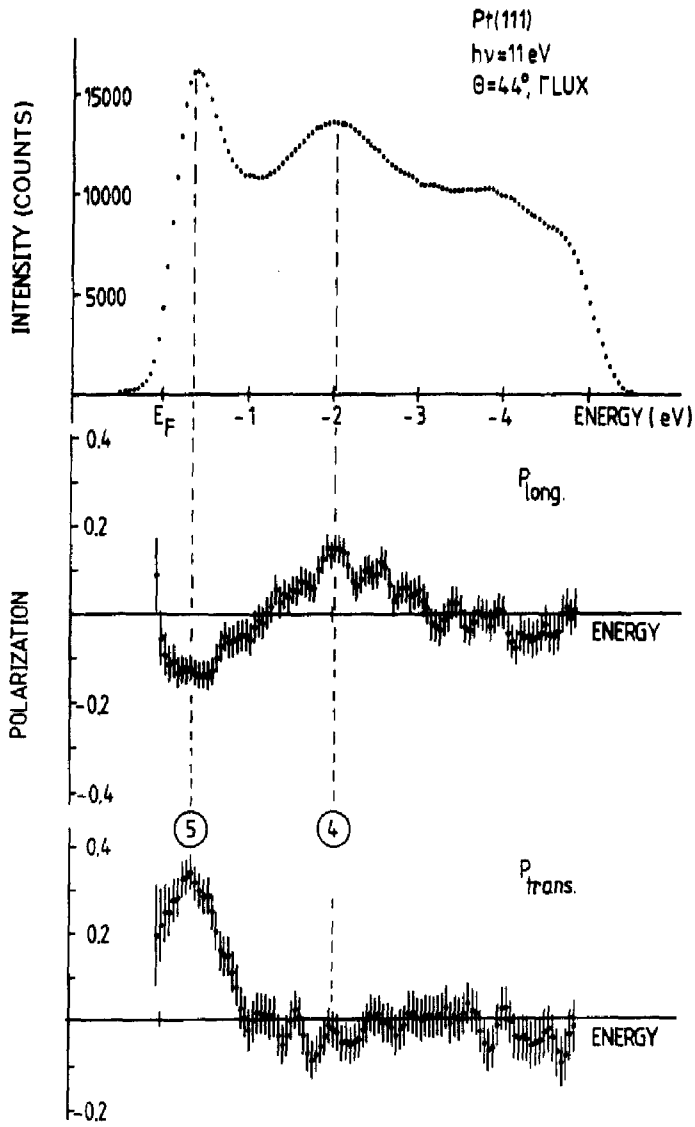

Fig. 14: Spectra of the intensity and the two inplane ESP components measured at normal incidence and a polar emission angle of 44° in the ΓLUX mirror plane of platinum (from Oepen 1984).

in the mirror plane. The two intensity peaks correspond to transitions from bands 5 and 4; obviously, the ESP vectors have different directions in the plane.

The variation of direction and magnitude of the ESP vector with emission angle and photon energy is illustrated in Fig. 15. The orientation of the ESP vector can deviate considerably from the direction of the photon spin (i.e. the surface normal). For the transition band 4 → 7 and an emission angle of 28° the electron and photon polarization vectors are nearly perpendicular to each other! There is evidence that this striking effect cannot be solely due to surface transmission, but the *excitation step* (within the three-step model)

produces a spin component *perpendicular* to the photon spin, similar to the atomic case (see Fig. 3). If surface transmission were dominant, the energy dependence should be much more pronounced than displayed in Fig. 15. Very recently Borstel (1985) has outlined the capability of such measurements to extract, in principle, the relative phases and magnitudes of distinct transition matrix elements. This would be a major step towards the complete characterization of electronic states in solids - the counterpart of the complete photoionization experiments in the gas phase (cf. 11.2.2).

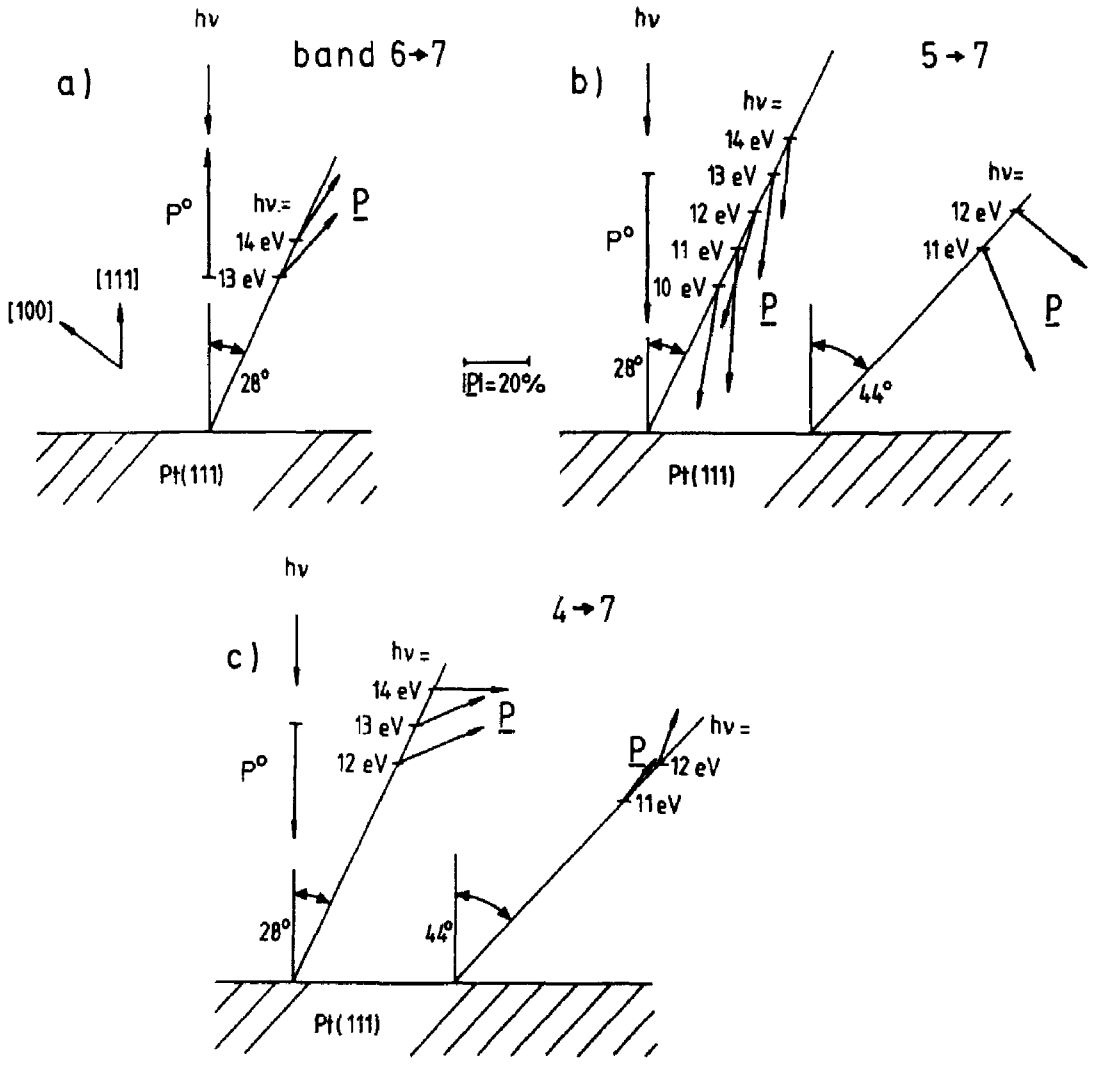

Fig. 15: Orientation and magnitude of the ESP vector in the [LUX mirror plane of Pt measured at two polar emission angles for various photon energies. Part a), b), and c) are transitions from bands no. 6, 5, and 4 (cf. Fig. 11), respectively. P° denotes the ESP vector for normal emission (from Oepen 1984).

11.6 Photoelectron Spinpolarization Spectroscopy of Physisorbed Rare Gases

The most recent progress in spin-resolved photoelectron spectroscopy was achieved for the case of adsorbate systems. This is a result of the development of electron storage rings which provide high photon intensities in the VUV range at very good ultrahigh vacuum conditions. Using the apparatus at BESSY (cf. 11.2) it has become possible to sample an ESP spectrum in less than one hour - a typical "lifetime" of a well-defined adsorbate overlayer. This opens up a wide field of possible investigations with a lot of fascinating new aspects.

11.6.1 Level Splitting

The symmetry operations which transform a wavefunction of an adsorbed atom into itself do no longer reflect the full symmetry of isotropic space but are restricted due to the adsorption geometry. Even for weakly bound (physisorbed) systems like the rare gases this reduction of symmetry by the presence of the surface may induce a splitting of energy levels. Consider, e.g., the $5p^6$ valence orbital of a free Xe atom (4p for Kr analogously). For these heavy atoms the spin-orbit interaction induces a strong mixing (hybridization) of the p_x, p_y and p_z orbitals such that the wavefunctions are eigenfunctions of j^2 and j_z. Starting from the atomic ground state $^1S_0$ (no spin-orbit interaction), photoemission of a valence electron leads to the p^5 configuration where angular- and spin momenta of the ion can couple to $^2P_{3/2}$ and $^2P_{1/2}$, briefly called the $p_{3/2}$ and $p_{1/2}$ hole states. Spin-orbit interaction in these final ionic states causes a splitting of 1.3 eV (0.6 eV for Kr).

Without magnetic interactions being present, the lowering of symmetry in the adsorbate system may result in a further splitting of $p_{3/2}$ into the $|m_j| = 3/2$ and $1/2$ sublevels. Indeed, Waclawski and Herbst (1975) observed a significant broadening of the corresponding peak in the photoelectron spectrum of xenon on tungsten, which they interpreted as the unresolved $|m_j|$ sublevel doublet split in the crystal field of the substrate-atom cores. On the other hand,

Matthew and Devey (1976) as well as Antoniewicz (1977) have pointed out that this model requires an unreasonably large positive charge on the surface atoms in order to produce the observed splitting. Instead, they proposed a splitting mechanism based upon image-charge screening which results in different relaxation shifts of the $p_{3/2}$ $|m_j| = 3/2$ and $1/2$ hole states. Finally, Horn et al. (1978) have measured a marked dispersion of the 5p-band in a Xe monolayer. From the measured dependence of the photoelectron intensities upon the angle of photon incidence they concluded that lateral interaction between adatoms is the dominant splitting mechanism (Scheffler et al. 1979). This explanation has been challenged repeatedly in recent years in the literature.

The nature of the *splitting mechanism* is closely related to the *energetic ordering* of the sublevels: substrate-induced relaxation effects cause the $|m_j| = 1/2$ level to have a lower binding energy than $|m_j| = 3/2$ (Matthew and Devey 1976), whereas the opposite is true if lateral interactions in the adlayer are responsible (Scheffler et al. 1979). Due to its unique capability of identifying orbital symmetries, ESP spectroscopy is a simple and reliable tool to clarify this question. On the basis of a theoretical model calculation for the photoemission from rare-gas adsorbates, Feder (1978) has shown that the ordering can be obtained from the ESP of the angle-integrated photocurrent if the dipole matrix elements are explicitly known. In the following, we outline a general group-theoretical treatment.

From LEED-patterns it is well known that at high coverage adsorbed rare-gas atoms form a hexagonally close-packed (hcp) overlayer. Hence, for normal emission (i.e. at the Γ point of the surface Brillouin zone) the symmetry group of the wave vector is C_{6v}. The wavefunctions are constructed of spatial and spin parts, with the first one transforming according to one of the representations of the single group. From the basis functions of C_{6v} tabulated by Koster et al. (1963, p.67) it is evident that p_z and $p_x p_y$ transform according to Δ_1 and Δ_5, respectively. Spin-orbit interaction is taken into account by reduction of the products with Δ_7 (generated by the

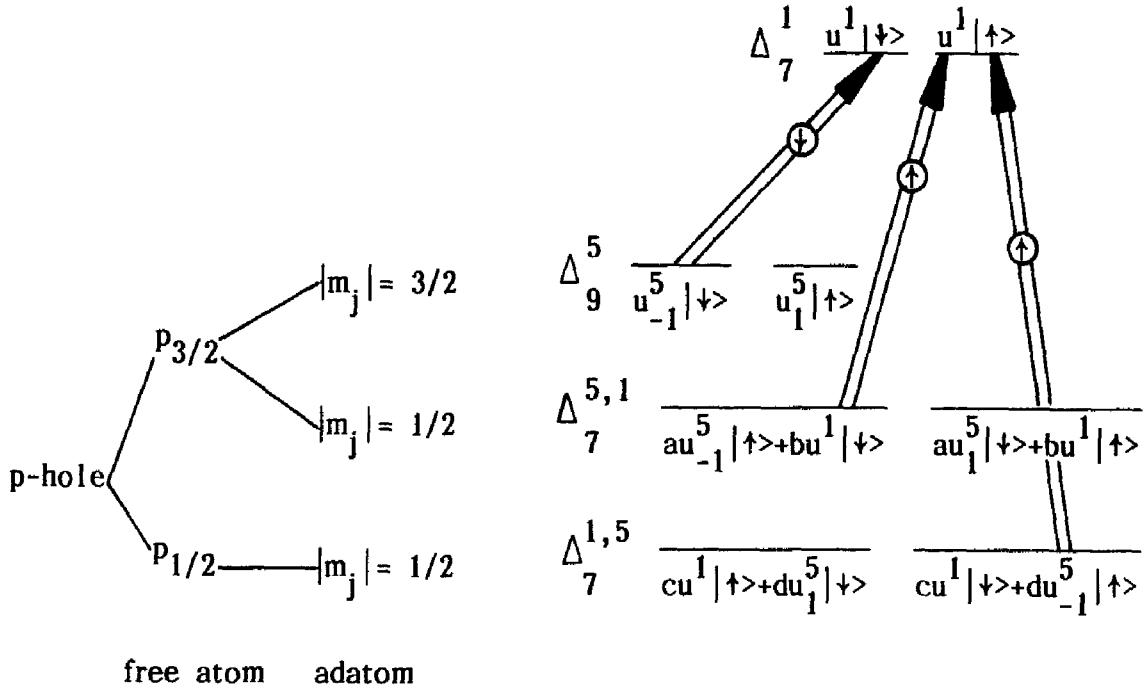

Fig. 16: Level scheme for transitions from the valence bands of adsorbed rare gases. Basis functions are from Koster et al. (1963), a-d being hybridization coefficients. Arrows indicate the transitions having non-vanishing matrix elements.

spinors $|\uparrow\rangle$ and $|\downarrow\rangle$), yielding* $\Delta_1 \times \Delta_7 = \Delta_7^1$ and $\Delta_5 \times \Delta_7 = \Delta_7^5 + \Delta_9^5$ (Koster et al. 1963, p. 68). Thus the 6-fold degeneracy of the p-orbital is lifted and a splitting occurs into three sublevels of 2-fold degeneracy (two of double group symmetry Δ_7 and one of Δ_9). In general, hybridization will cause a mixing of Δ_7^5 and Δ_7^1 wavefunctions (p_{xy}-p_z hybrids $\Delta_7^{5,1}$), whereas Δ_9^5 is of a single symmetry type (pure p_{xy}).

Fig. 16 shows the resulting level scheme. In order to derive the ESP of photoelectrons emitted by circularly polarized light we follow the way described by Meier and Pescia (1984). For normal incidence (propagation along -z) the radiation operator for circularly polarized light (σ^-) transforms as x + iy (equivalent to $-i(s_x+is_y)$)

* According to common convention, the superscript (subscript) indicates the corresponding single (double) group representation.

and hence according to the basis function u_1^5 of Δ_5. The final state is assumed to be a plane wave with wave vector along the z direction transforming as Δ_7^1 (in the present geometry equivalent to a spherically symmetric s-wave). From the transition scheme one can easily see that all dipole matrix elements for optical transitions have the form $\langle f|Op.|i\rangle = \langle u^1|u_1^5|u^1 \text{ or } u_1^5 \text{ or } u_{-1}^5\rangle$ where it was used that the dipole operator acts only on the orbital part of the wavefunctions. Since the reduction of Δ_5 (light operator) x Δ_1 (initial state) does not contain Δ_1 (final state), the transition from a band with pure Δ_1 orbital symmetry is dipole-forbidden. The orbital part of the final-state wavefunction u^1 expressed in terms of products of basis functions Δ_5 x Δ_5 reads $u^1 = \frac{1}{\sqrt{2}}(u_{-1}^5 v_1^5 + u_1^5 v_{-1}^5)$ (Koster et al. 1963, p. 69). Consequently the only non-vanishing matrix element is $\langle u^1|u_1^5|u_{-1}^5\rangle \neq 0$. Finally, due to the orthogonality of the spin functions ($\langle\uparrow|\downarrow\rangle = 0$) only the three transitions denoted by arrows are allowed for circularly polarized light, yielding the ESP values:

$$P = \begin{cases} -1 \text{ for } p_{3/2} \ |m_j| = 3/2 \\ +1 \text{ for } p_{3/2} \ |m_j| = 1/2 \text{ and for } p_{1/2} \end{cases}$$

These very general arguments are based upon *symmetry properties* only, they hold irrespective of the magnitude of the matrix elements, the hybridization coefficients a-d (as long as a and d $\neq$ 0) and even irrespective of the physical nature of the splitting mechanism. It is thus not surprising that one gets the same results by using the angular part of the *atomic* wavefunctions Y_ℓ^m (analogously to the procedure described in Kessler 1976) (Schönhense et al. 1985a). Two spinresolved photoelectron spectra are shown in Fig. 17. For Xe and Kr the peak at lowest binding energy (peak 1) has nearly complete negative ESP which, according to the above arguments, corresponds to the $p_{3/2}$ $|m_j| = 3/2$ hole state, whereas peak 2 and 3 (here for Kr only) are highly positively polarized, i.e. $|m_j| = 1/2$. This result confirms the peak assignment given by Horn et al. (1978), which

indicates that the splitting is caused by *lateral adatom interactions*. The high ESP of over ±85 % exceeds all values previously found for other nonmagnetic solid-state systems. It is interesting, to compare the results with the free-atom case: The degeneracy of the two $p_{3/2}$ sublevels with opposite sign of polarization *diminishes* the ESP to $P \simeq -0.5$ since for free ions the intensity ratio between the $|m_j| = 3/2$ and 1/2 channels is close to 3 (exactly 3 in the LS-coupling approximation). For the non-split $p_{1/2}$ level the complete positive polarization predicted by group theory has also been observed in a recent gas-phase experiment (Heckenkamp et al. 1984) as shown in Fig. 4.

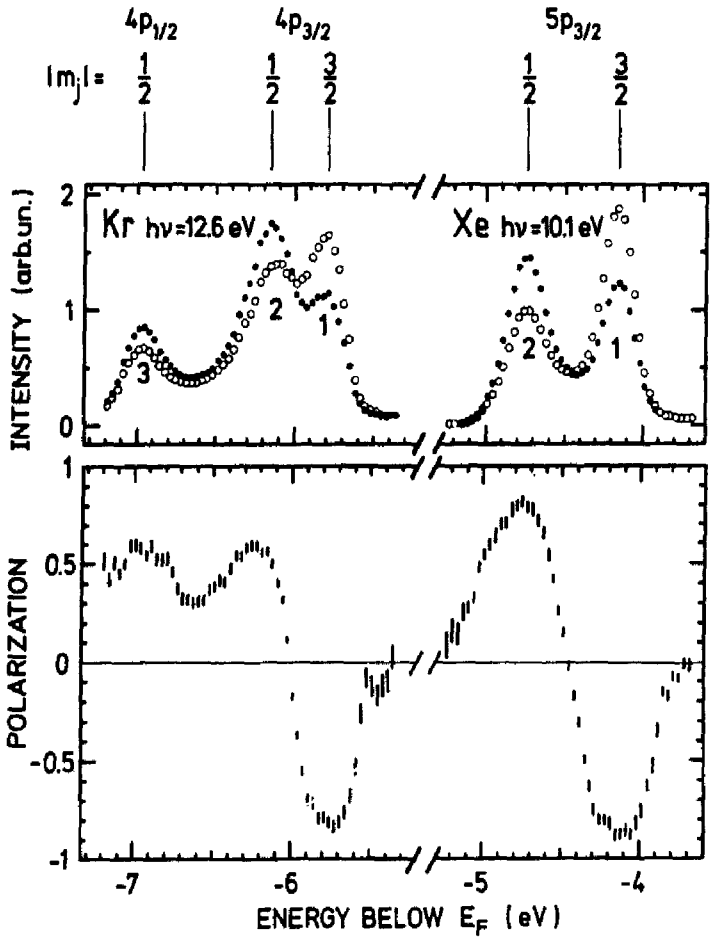

Fig. 17: ESP spectra of Kr and Xe monolayers. The measured intensity asymmetry in the Mott detector (upper part) yields the ESP (lower part) (from Schönhense et al. 1985a).

11.6.2 Resonance Behavior of the Spin Polarization

At photon energies just above the Xe 5p and Kr 4p thresholds the photoemission intensities are strongly enhanced so that for monolayer coverage the adsorbate photoemission can exceed the Pt d-band emission (close to E_F) by two orders of magnitude (cf. Schönhense et al. 1985a). In order to study the threshold behavior in more detail, the energy variation of intensity and ESP of the three Xe 5p-derived peaks has been measured as function of photon energy (summarized in Figs. 18-20) using circularly polarized synchrotron radiation and the apparatus shown in Fig. 2. Results have been obtained (i) for the commensurate $\sqrt{3} \times \sqrt{3}$ (R 30°) overlayer on the Pt(111) face, (ii) for the incommensurate hexagonally close-packed (hcp) monolayer on Pt(111) and (iii) for the hcp monolayer on the basal plane of (natural single-crystal) graphite. Note that the intensity scales (in arbitrary units) are

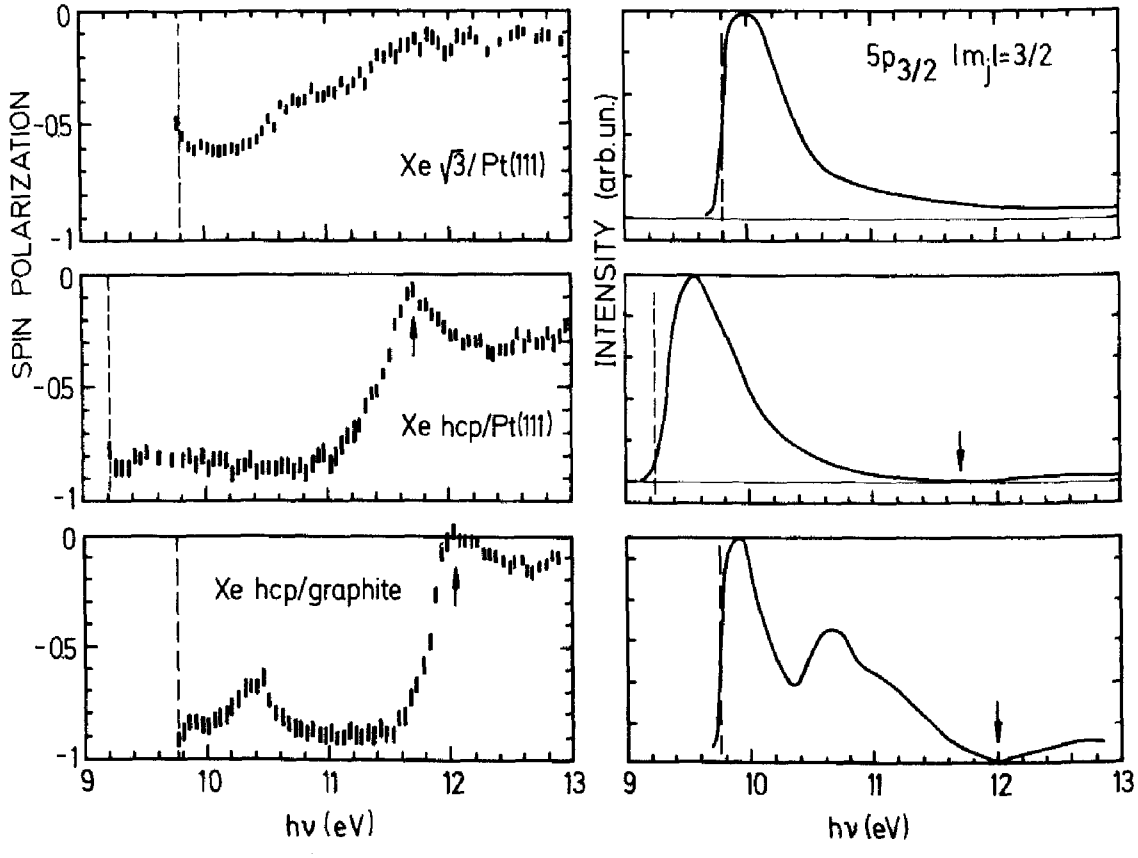

Fig. 18: Spectral variation of ESP (left) and corresponding intensity (right) for the Xe $5p_{3/2}$ $|m_j|$ = 3/2 hole state at normal incidence and emission (from Schönhense et al. 1985a and b).

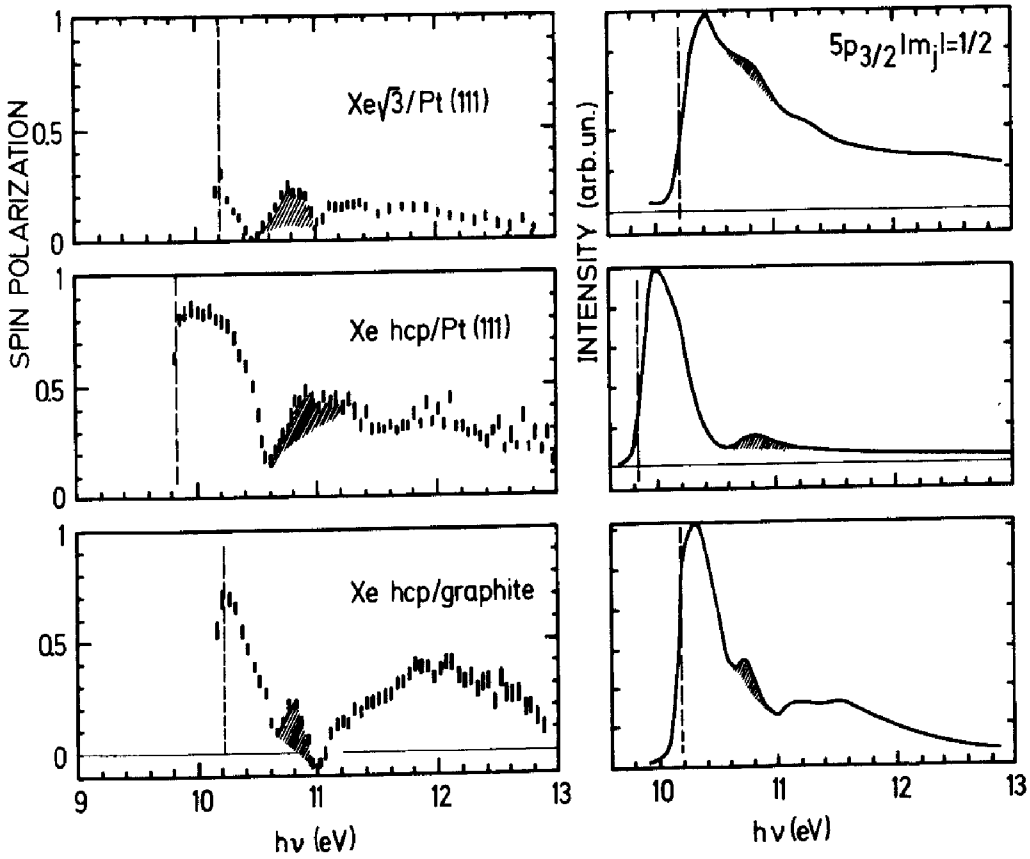

Fig. 19: The same as Fig. 18 but for Xe $5p_{3/2}$ $|m_j| = 1/2$

different from each other. It is advantageous to plot the data versus photon energy, because this representation is well-defined independent of workfunction changes. The figures reveal that the intensities of all peaks are strongly enhanced just above their thresholds (dashed lines, binding energies with respect to the vacuum level) but fall off rapidly towards higher energies within less than one eV. All ESP curves* show the signs predicted by group theory (see 11.6.1) but instead of having constant values ±1, they exhibit pronounced variations with photon energy! Evidently, there are important effects which were not included in the above symmetry considerations.

* It was found that the adsorbate layer strongly influences the substrate spectrum (cf. section 11.7). Therefore no reliable estimation of an underlying background of unpolarized secondary electrons could be made and hence the uncorrected ESP values are given.

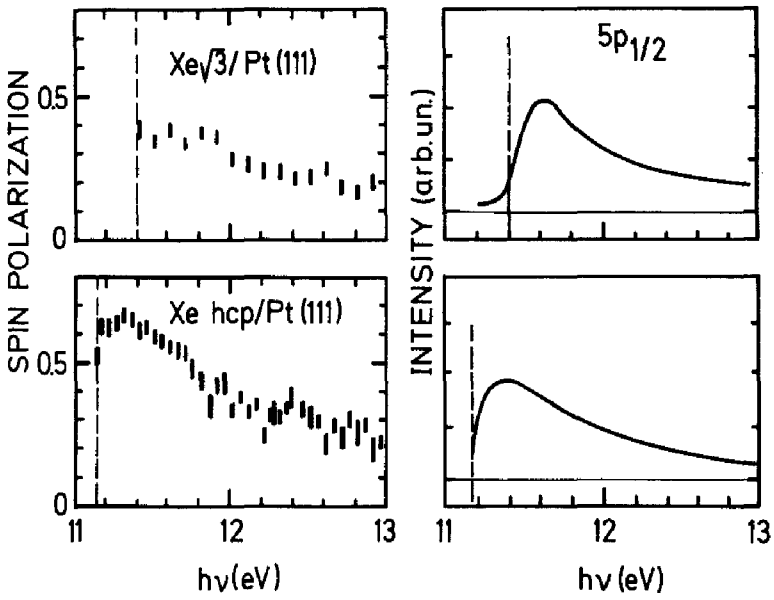

Fig. 20: The same as Fig. 18 but for Xe $5p_{1/2}$

One important mechanism which leads to strong variations of electron spinpolarizations and intensities (the so-called "dynamical" parameters) in near-threshold photoemission from *free* rare-gas atoms is *autoionization*. Autoionization resonances occur whenever discrete Rydberg-type excitations interact with a degenerate photoemission continuum leading to the well-known asymmetric Beutler-Fano profiles. In the particular case of xenon atoms the 5p → ns and 5p → nd series, converging to the $Xe^+ {}^2P_{1/2}$ ionization threshold give rise to strong ESP and intensity features between the fine-structure split $^2P_{3/2,\ 1/2}$ thresholds (cf. Heinzmann et al. 1979b). Such an autoionizing transition in Xe adatoms is most probably the origin of the hatched feature in the ESP and intensity curves of the $p_{3/2}$ $|m_j| = 1/2$ channel (Fig. 19), because it appears at nearly the same photon energy for all Xe layers studied independent of the substrate and the coverage.

The most surprising resonance features have recently been observed *below* the adsorbate photoemission thresholds. Very narrow Xe 5p → 6s and Kr 4p → 5s resonance transitions occur in the adsorbate phase. They show almost no relaxation shift compared to the gas phase and persist even in the submonolayer regime! Fig. 21 shows the results for Xe on graphite. The resonances were detected via spin-resolved spectroscopy of the electrons just above the low-energy cut-

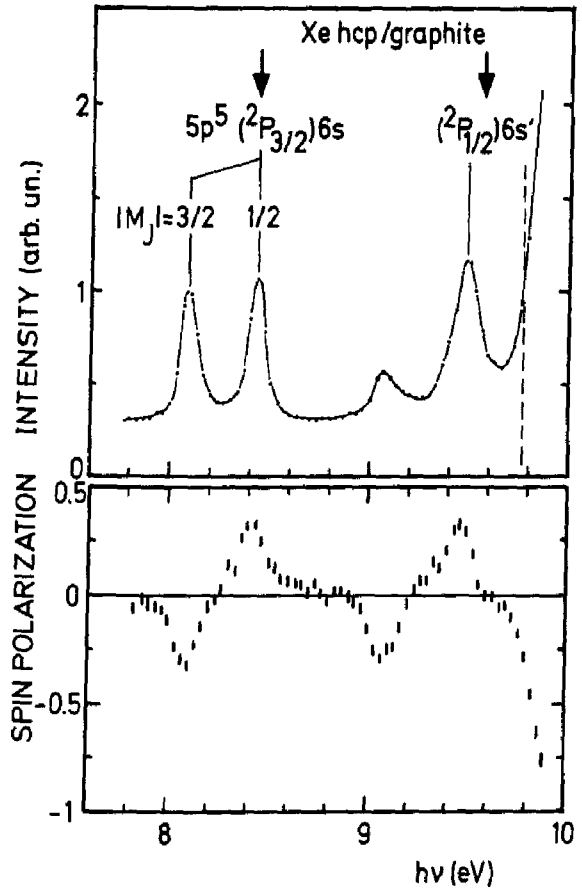

Fig. 21: Resonant electron emission from a xenon monolayer on graphite; arrows indicate the 6s and 6s' resonance-line positions for *free* atoms (from Schönhense et al. 1985b).

off of the spectrum, which are emitted due to a subsequent relaxation mechanism (probably a Penning-type decay). The ESP again provided a quantum-number labelling of the peaks according to 11.6.1 and furthermore clarified the nature of the decay mechanism observed (cf. Schönhense et al. 1985b). Note that the Xe* $5p^5(^2P_{3/2})6s$ excited level is split into $|M_J|$ = 3/2 and 1/2 (core-) sublevels although the Xe* complex is electrically neutral, i.e. no image-charge screening should occur. The resonances in the two-dimensional overlayer are closely related to the surface excitons in rare-gas crystals observed by Saile et al. (1976). The feature at 9.1 eV might well be the n = 2 exciton of the atomic-line derived 8.1 eV-peak. Owing to its negative ESP it is evidently associated with the $|M_J|$ = 3/2 core.

11.6.3 Influence of Substrate, Overlayer Structure and 2D Phase Transitions

An especially interesting point in adsorbate physics is the feasibility to vary the substrate crystal and in some cases also the adatom-adatom spacing via the coverage. For the weakly bound rare-gas atoms, which constitute a model case of matter in a state between gas and solid, one can thereby probe the influence of an increasing valence-orbital overlap on energy levels and photoemission dynamics.

Fig. 18 shows one striking difference between the commensurate Xe $\sqrt{3}$ phase on Pt(111) and the incommensurate hcp phases: whereas for $\sqrt{3}$ (Xe-Xe spacing 4.8 Å) the photoemission intensity is always different from zero, the $p_{3/2}$ $|m_j| = 3/2$ peak *vanishes* for both hcp layers (Xe-Xe spacing 4.4 Å), leading to sharp minima in the ESP curves (arrows). This different behavior has a remarkable effect on the photoelectron spectra. At $h\nu = 11.7$ eV the spectrum of Xe $\sqrt{3}$ / Pt(111) clearly shows three Xe 5p-derived peaks; on adding a little more Xe, however, the first peak falls off until at monolayer saturation it has almost completely vanished (see Schönhense et al. 1985a). Hence, in the threshold region the peak heights may even depend reversely on the coverage! Another obvious difference between the two Xe phases on Pt(111) is the position of the photoemission thresholds (dashed lines in Figs. 18-20). This is essentially a consequence of the increased valence-orbital overlap in the hcp layer; the workfunction difference is only less than 100 meV. Furthermore, the ESP values for Xe $\sqrt{3}$ are considerably lower than for hcp - especially in the $p_{3/2}$ $|m_j| = 1/2$ channel (Fig. 19). The unpolarized background of secondaries can only partly account for this effect.

On the other hand, Xe hcp monolayers on such different substrates as platinum and graphite show marked differences in the ESP and intensity curves, too. Additional features occur on the graphite surface: (i) a strong intensity structure between 10 and 11 eV in the $p_{3/2}$ $|m_j| = 3/2$ channel (Fig. 18), also visible in the ESP and (ii) weak features between 11 and 12 eV in the $|m_j| = 1/2$ channel (Fig. 19).

A possible reason could be that the influence of the substrate on the Xe adatoms is weaker for graphite than for Pt(111). Consequently, more resonant transitions could persist on graphite. This interpretation is supported by the fact that the width of the hatched features is significantly smaller for graphite, i.e. less disturbed, than for Pt.

Besides the commensurate-incommensurate phase transition, also a 2D-liquid-solid phase transition is intensely studied at present (Poelsema et al. 1983, Wandelt 1985). It is to be expected that ESP spectroscopy can give important insights into the level splitting mechanism in the liquid phase at low coverage and hence for negligible valence-orbital overlap. Such investigations are in progress.

11.7 Adsorbate-Induced Changes in Substrate ESP Spectra

Besides the spinpolarization effects in photoemission from adsorbate levels, discussed in the preceding section, also the ESP of those photoelectrons originating from the substrate bands may show significant adsorbate-induced changes. Only very recently have such changes been observed and our knowledge of the interactions experienced by the photoelectron when travelling across an adsorbate layer is still rather sparse.*

Early experiments on cesiated GaAs never gave a clear indication for depolarization by spin-exchange scattering of photoelectrons at the Cs atoms on the surface (Pierce and Meier 1976). This result was no surprise, because for submonolayer coverages the Cs atom is ionized and thus has rare-gas electron configuration with zero spin leading to a very small spin-exchange constant. The situation becomes quite different if the adatoms carry magnetic moments. Then even a single paramagnetic monolayer may have a depolarizing effect as high as 50 % (Helman and Siegmann 1973). Meier et al. (1982b and 1984) performed a systematic study of the ESP of photoelectrons excited by circularly polarized light in Ge covered with variable amounts of Ni, Gd, Ce and Au. The mean free paths for spin-flip scattering turned out to lie between a few Ångstroms only for the magnetic materials (3.2 Å for Ce) and > 50 Å for Au, having no magnetic moment (cf. chapter 10).

A lot of details of the adsorbate-induced changes have been revealed in a recent energy- and angle-resolved ESP study (Eyers et al. 1985). Fig. 22 shows some selected intensity spectra of the adsorbate system xenon on platinum (111) for two different photon energies and various coverages. The spectra of the clean substrate (a) show the pronounced peaks due to the direct interband transitions along the Γ-L direction of Pt as discussed in section 11.3. The series of spectra

* The case of magnetic materials, where even nonmagnetic adsorbate overlayers strongly influence the magnetism of the surface (Meier et al. 1975 and 1982a) will not be discussed in this context.

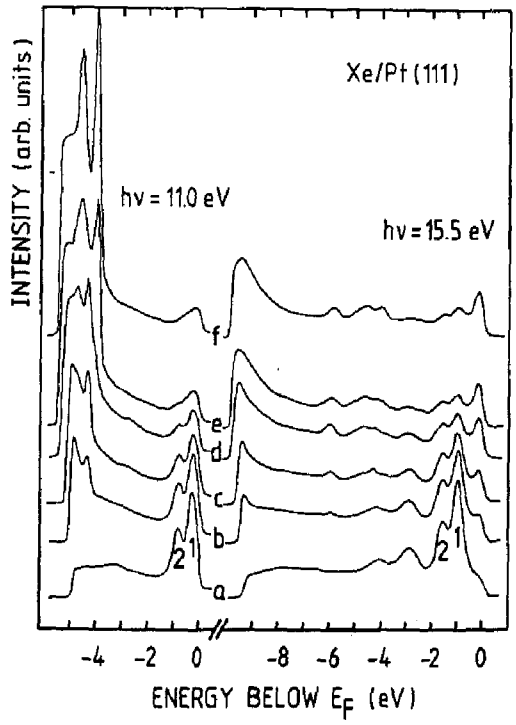

Fig. 22: Photoelectron spectra of Pt(111) for normal incidence and normal emission taken at various Xe coverages between (a) clean substrate and (f) complete incommensurate hcp monolayer (from Eyers et al. 1985).

at hν = 11 eV lies in the energy region of the anomalously intense photoemission from the Xe valence orbitals. Along with the strongly increasing $p_{3/2}$ $|m_j|$ = 3/2, 1/2 peaks on the left, the Pt photoemission intensity of peaks 1 and 2 (bands 6 and 5, Fig. 5) is drastically reduced with increasing Xe coverage. For the completed commensurate $\sqrt{3}$ overlayer (spectrum d) and the saturated incommensurate hcp monolayer (spectrum f) the Pt peak heights have decreased by factors of about 2.5 and 4, respectively.

At hν = 15.5 eV (right series) photoemission from Xe is much weaker: even at full monolayer coverage (f) the Pt peaks still exceed the Xe peaks (located between -6 and -4 eV below E_F). Again, the Pt peak heights are reduced by roughly the same factors as observed for hν = 11 eV. However, in addition an adsorbate-induced new peak just below the Fermi level (0.25 eV below E_F) arises, which was only visible as a shoulder in the 15.5 eV spectrum of the clean substrate (a). The same behavior, i.e. a marked decrease in the d-band transition intensities and an enhancement of the peak just below E_F was also found for krypton overlayers. The main part of the observed decrease

is clearly caused by inelastic scattering processes at the adatoms as is evident from the rise of the broad feature of secondaries at the low-energy cut-off of the 15.5 eV spectra.

One plausible explanation of the adsorbate-enhanced peak can be given in terms of photoelectron scattering, as well. The band just below E_F along the Q direction (cf. Fig. 5), which shows only a weak dispersion, gives rise to a maximum in the total density of states just below E_F. It is likely that part of the emission from this band is elastically scattered on the adatoms into the normal emission direction. This explanation is supported by the experimental facts that the new peak does not show a measurable dispersion (cf. Eyers et al. 1985) and its ESP is very low (< 10 %). Neglecting hybridization effects, interband transitions along the Q-line should yield unpolarized electrons.

Fig. 23 shows the ESP of peaks 1 and 2 as function of photon energy for the clean Pt(111) substrate and for Pt with a complete $\sqrt{3} \times \sqrt{3}$ (R 30°) overlayer of Xe atoms. Throughout the energy range studied a significant depolarization due to the Xe layer occurs. It must be pointed out that the effect appears even more pronounced if one takes the temperature dependence of the ESP into account: at T = 50 K (corresponding to the full circles) the ESP of the clean surface (open circles) lies close to ±70 % (cf. Fig. 7c). The depolarizations of both peaks show a similar systematic photon-energy dependence. Towards lower energies the ESP is reduced more and more. However, it is somewhat problematic to interpret this variation quantitatively in terms of an energy-dependent exchange constant, because below $h\nu$ = 12 eV the new adsorbate-induced peak discussed above partly overlaps with peaks 1 and 2. Such an underlying contribution of essentially unpolarized electrons would appear as an additional depolarizing mechanism. For a complete Xe hcp monolayer the ESP was found to be less than ±15 % throughout the energy range of Fig. 23.

The first results of adsorbate-induced changes in substrate ESP spectra cannot be explained in terms of spin-flip scattering alone.

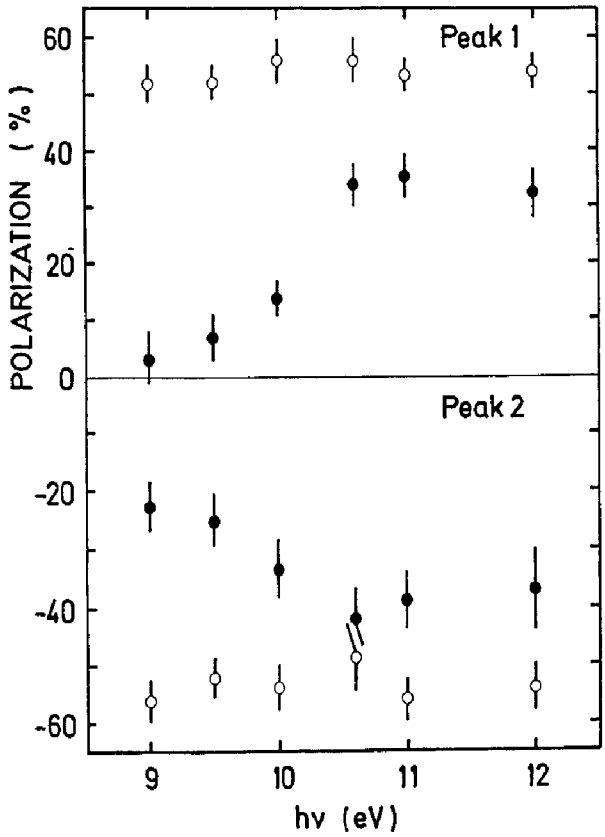

Fig. 23: Photoelectron polarization of peaks 1 and 2 of Pt(111) versus photon energy for clean Pt (T = 300 K, open circles) and for Pt covered by a complete $\sqrt{3}$ layer of Xe (T = 50 K, full circles) (from Eyers et al. 1985).

Even submonolayer coverages of Xe and Kr atoms can cause considerable changes which become observable in energy- and emission-angle resolving experiments. Elastic and inelastic photoelectron scattering processes, modifications of the substrate band structure in the surface region as well as the presence of surface states are strongly related to the structure and coverage of adsorbate overlayers. Systematic studies of high-resolution photoelectron intensity- and ESP-spectra together with quantitative theoretical calculations should give a deeper insight into these phenomena. Of particular interest are the chemisorbed (i.e. strongly bound) adsorbate systems, the study of which has just been started.

Acknowledgements:

We would like to thank A. Eyers, U. Frieß and F. Schäfers for their engagement and wealth of ideas in performing the experiments at BESSY. Thanks are due to N. Böwering for a critical reading of the manuscript. The friendly cooperation with G. Borstel, K. Hünlich, J. Kirschner, F. Meier, N. Müller, H.P. Oepen and with our colleagues from the Surface Science Department of the Fritz-Haber-Institut and the BESSY staff is gratefully acknowledged. The experiments were supported by the BMFT, the MPG, the KFA, and BESSY.

References:

Ackermann B and Feder R 1985, Solid State Commun. 54, 1077

Andersen O K 1970, Phys. Rev. B2, 883

Antoniewicz P R 1977, Phys. Rev. Lett. 38, 374

Borstel G 1985, Solid State Commun. 53, 87

Borstel G and Wöhlecke M 1981, Phys. Rev. B24, 2321

Borstel G and Wöhlecke M 1982, Phys. Rev. B26, 1148

Cherepkov N A 1973, Zh. Eksp. Teor. Fiz. 65, 933
(Sov. Phys. JETP 38, 463 (1974))

Christensen N E 1981, Solid State Commun. 37, 57

Christensen N E and Seraphin B 1971, Phys. Rev. B4, 3321

Christensen N E and Feuerbacher B 1974, Phys. Rev. B10, 2349

Eyers A, Heckenkamp Ch, Schäfers F, Schönhense G and Heinzmann U
1983, Nucl. Instr. Meth. 208, 303

Eyers A, Schönhense G, Friess U, Schäfers F and Heinzmann U 1985,
Surface Sience (in press)

Eyers A, Schäfers F, Schönhense G, Heinzmann U, Oepen H P, Hünlich K,
Kirschner J and Borstel G 1984, Phys. Rev. Lett. 52, 1559

Fano U 1969, Phys. Rev. 178, 131

Feder R 1977, Solid State Commun. 21, 1091

Feder R 1978, Solid State Commun. 28, 27

Ginatempo B, Durham P J, Gyorffy B L and Temmerman W M 1985,
Phys. Rev. Lett. 54, 1581

Heckenkamp Ch, Schäfers F, Schönhense G and Heinzmann U
1984, Phys. Rev. Lett. 52, 421

Heckenkamp Ch, Schäfers F, Schönhense G and Heinzmann U
1985, Phys. Rev. A (in press)

Heinzmann U 1978, J. Phys. B11, 399

Heinzmann U 1980a, Appl. Opt. 19, 4087

Heinzmann U 1980b, J. Phys. B13, 4353 and 4367

Heinzmann U, Kessler J and Lorenz J 1970, Phys. Rev. Lett. 25, 1325

Heinzmann U, Schönhense G and Kessler J 1979a,
Phys. Rev. Lett. 42, 1603

Heinzmann U, Jost K, Kessler J and Ohnemus B
1972, Z. Phys. 251, 354

Heinzmann U, Osterheld B, Schäfers F and Schönhense G
1981, J. Phys. B14, L79

Heinzmann U, Schäfers F, Thimm K, Wolcke A and Kessler J 1979b,
J. Phys. B12, L679

Helman J S and Siegmann H C 1973, Solid State Commun. 13, 891

Horn K, Scheffler M and Bradshaw A M 1978, Phys. Rev. Lett. 41, 822

Kessler J 1976, "Polarized Electrons", Springer-Verlag, Berlin

Kirschner J, Feder R and Wendelken J F 1981, Phys. Rev. Lett. 47, 614

Koster G F, Dimmock J O, Wheeler R G and Statz H 1963,
"Properties of the Thirty-Two Point Groups", MIT Press,
Cambridge (Mass)

Koyama K and Merz H 1975, Z. Phys. B20, 131

Lampel G 1968, Phys. Rev. Lett. 20, 491

Lee C M 1974, Phys. Rev. A10, 1598

Leschik G, Courths R, Wern H, Hüfner S, Eckardt H and Noffke J
1984, Solid State Commun. 52, 221

MacDonald A H, Daams J M, Vosko S H and Koelling D D 1981,
Phys. Rev. B23, 6377

Matthew J A D and Devey M G 1976, J. Phys. C9, L413

Meier F and Pescia D 1981, Phys. Rev. Lett. 47, 374

Meier F and Pescia D 1984, in "Optical Orientation",
ed. by Meier F and Zakharchenya B P, North-Holland, Amsterdam

Meier F, Pierce D T and Sattler K 1975, Solid State Commun. 16, 401

Meier F, Pescia D and Schriber T 1982a, Phys. Rev. Lett. 48, 645

Meier F, Pescia D and Baumberger M 1982b, Phys. Rev. Lett. 49, 747

Meier F, Bona G L and Hüfner S 1984, Phys. Rev. Lett. 52, 1152

Mills K A, Davis R F, Kevan S D, Thornton G, and Shirley D A 1980,
Phys. Rev. B22, 581

Mueller F M, Garland J W, Cohen M H and Bennemann K H 1971, Ann. Phys. (N.Y.) 67, 19

Oepen H P 1984, Thesis Technische Universität Aachen (to be published)

Oepen H P, Hünlich K and Kirschner J 1984, BESSY Jahresbericht p. 239

Oepen H P, Hünlich K, Kirschner J, Eyers A, Schäfers F, Schönhense G and Heinzmann U 1985, Phys. Rev. B31, 6846 - and to be published

Pierce D T and Meier F 1976, Phys. Rev. B13, 5484

Poelsema B, Verheij L K and Comsa G 1983, Phys. Rev. Lett. 51, 2410 and Surface Science (in press)

Reyes J and Helman J S 1977, Phys. Rev. B16, 4283

Saile V, Skibowski M, Steinmann W, Gürtler P, Koch E E and Kozevnikov A 1976, Phys. Rev. Lett. 37, 305

Schäfers F, Heckenkamp Ch, Schönhense G and Heinzmann U 1985, 2. Europ. Conf. Atomic Mol. Physics, Amsterdam, Book of abstracts

Scheffler M, Horn K, Bradshaw A M and Kambe K 1979, Surf. Sience 80, 69

Schönhense G 1980, Phys. Rev. Lett. 44, 640

Schönhense G, Eyers A, Friess U, Schäfers F and Heinzmann U 1985a Phys. Rev. Lett. 54, 547

Schönhense G, Eyers A and Heinzmann U 1985b - to be published

Waclawski B J and Herbst J F 1975, Phys. Rev. Lett. 35, 1594

Wandelt K 1985, ECOSS 7, Aix-Marseille, Book of abstracts p. 343 and private communication

Wöhlecke M and Borstel G 1981, Phys. Rev. B23, 980

Zürcher P and Meier F 1979, J. Appl. Phys. 50(3), 2097

Zürcher P, Meier F and Christensen N E 1979, Phys. Rev. Lett. 43, 54